SALINITY DEPENDENCE OF SHALY SAND PARAMETERS FROM MEMBRANE POTENTIAL MEASUREMENTS

By

H. H. Yuan

Shell Development Company

(now with Shell Western E&P Inc.)

Abstract

The Yuan-Diederix equation relates the conductivity of a brine saturated rock sample to the brine conductivity and membrane and Nernst potentials for the sample for a given salinity contrast. It can be used for determining the salinity dependence of shaly sand parameters because the equation can be determined from parameters measured at essentially one salinity. This paper applies membrane potential measurements and the Yuan-Diederix equation to describe the salinity dependence of the clay conductivity, C_e, the shaly sand formation resistivity factor, F*, the shaly sand lithology exponent, m*, and the equivalent quadrature conductance, λ.

Data from the Waxman-Smits Group 2 samples for which conductivity and membrane potential data have been simultaneously measured allow the determination of C_e, F* and m* as a function of salinity. The clay conductivity generally decreases with decreasing salinity. Accordingly, any shaly sand model should incorporate a salinity dependent clay conductivity as the Waxman-Smits model does. When the clay conductivity is smaller than the brine conductivity, F* is found to be constant, verifying that the Waxman-Smits assumption of constant F* is valid. When the clay conductivity is larger than the brine conductivity, F* generally increases with decreasing salinity implying that the Waxman-Smits assumption of constant F* is not always valid. A consequence of salinity-dependent F* is that membrane potential measurements may be necessary for cases where the clay conductivity exceeds the brine conductivity. In this salinity range, m* also increases. The salinity effects are much greater for samples containing montmorillonite.

New simultaneous conductivity, membrane potential and induced polarization data are reported here for a set of very shaly sandstones which confirm the salinity dependence of C_e, F* and m*. The new data are used also to determine the salinity dependence of the equivalent quadrature conductance, λ. The results agree very well with Vinegar-Waxman induced polarization data on shaly sands. It is found that induced polarization measurements also directly yield the clay conductivity.

1. Introduction

Waxman and Smits[1] (WS) describe the conductivity behavior of brine saturated shaly sands as follows:

$$C_o = (C_w + C_e)/F^* \qquad (1)$$

where C_o is the conductivity of the brine saturated shaly sand,
C_w is the brine conductivity,
C_e is the clay conductivity and
F^* is the shaly sand formation resistivity factor.

In the WS interpretation of equation (1) the salinity dependence of C_e is determined by assuming F^* to be constant and equal to the reciprocal slope of the straight line (high salinity) portion of C_o-C_w plot. Shaly sand C_o-C_w plots show non-linearity at low salinities. Once F^* is obtained, C_e is determined from C_o and C_w.

The clay conductivity, C_e, is expressed by WS as the product of the equivalent counterion conductance, B, and the cation exchange capacity, Q_v. The factor, B, is dependent upon salinity, temperature and cation type and in general is independent of the particular sample of interest while Q_v is a measure of the sample shaliness. The salinity dependence of B is determined from a set of C_o-C_w measurements to determine C_e and then additional Q_v measurements yield corresponding B values. However, it has been found recently that B also depends on clay geometry[2,3] and therefore can depend on the sample of interest. This is because the factor, Q_v, is determined by disaggregating the sample and performing conductometric titration on the crushed sample. Effects of clay geometry on clay conductivity appear in the B factor because effects of clay geometry on Q_v have been strongly diminished.

Membrane potential measurements also yield the clay conductivity and because membrane potential measurements are performed on the sample with the clay geometry intact, the clay conductivity correctly incorporates clay geometric effects. Cation exchange capacity from membrane potential is denoted as Q_{ve} for effective cation exchange capacity. The effect of clay geometry is properly incorporated in Q_{ve} and thus the B factor becomes independent of clay geometry when Q_{ve} is used to determine B. Moreover, the determination of clay conductivity is independent of F^*. By using membrane potential and conductivity measurements performed at essentially a single salinity, the need for high salinity data to determine F^* is eliminated.

The main objective of this paper is to describe the salinity dependence of shaly sand parameters based on membrane potential measurements. Another objective of the paper is to introduce a second data set where conductivity, membrane potential and induced polarization measurements were simultaneously made. The paper focusses on the analysis of experimental data although limited discussion of shaly sand models is given. However, reference is made to the WS model because it is on their Group 2 data that this paper is largely based. Discussion is also devoted to the Vinegar-Waxman model of quadrature conductivity of shaly sands because of the phase angle measurements presented here.

Many shaly sand models exist and have been reviewed by Worthington[4]. More recent publications on membrane potentials and conductivity of shaly sands have also appeared. Steward and Burck focussed on improving Q_v determination from membrane potential measurements[5]. Silva and Bassiouni published a theory of membrane potential of shaly sands[6] based on the dual water

model[7] but they focussed on predicting membrane potentials of shaly sands from Q_v data as opposed to the more important reverse step of inferring clay conductivity from membrane potential measurements. Cohen and Radke used details of clay morphology to build a model of conductivity of shaly sands[8]. Stenson and Sharma[9] attempted a theory of conductivity and electrokinetics (including membrane potentials) based on capillary tubes lined with clays. Hardwick[10] introduced a shale parameter based on low salinity conductivity which has the advantage of incorporating clay geometry by using conductivity and not Q_v but has the disadvantage of being based on formation resistivity factor, which may be salinity dependent (see below). Sen agreed with the importance of clay geometry on clay conductivity[11] and verified the Yuan-Diederix equation for clay conductivity from membrane potential measurements[12].

The paper is organized as follows. The next section gives relevant theory of membrane potential and induced polarization of shaly sands. Section 3 describes the experimental aspects of conductivity and membrane potential measurements. Section 4 describes the salinity dependence of the clay conductivity, C_e and the salinity dependence of the effective cation exchange capacity, Q_{ve}. The salinity dependence of F* is described in section 5, while Section 6 describes the salinity dependence of m* as a consequence of salinity dependence in F*. Induced polarization parameters are determined in section 7. Section 8 contains a discussion and Section 9 concludes the paper.

Throughout the paper, salinity will be characterized by its conductivity, C_w (in mmhos/cm) or its resistivity, R_w (in ohm cms) and is limited to sodium chloride brines at room temperature.

2. Theory of Shaly Sand Parameters

2a. Membrane Potential Theory

Smits[13] derived an integral equation for membrane potential which when expressed as the difference between the measured membrane potential, E_m, and the liquid junction potential, E_t, becomes:

$$\Delta U = E_m - E_t = \frac{-2RT}{F} \int_{m_1}^{m_2} \frac{C_e}{C_w + C_e} (1 - t_{Na}) \, d \ln(m\gamma\pm) \qquad (2)$$

where $\frac{2RT}{F}$ is a thermodynamic constant and equal to 51.4mV at 25 degrees C,

t_{Na} is the sodium Hittorf transport number,
$m\gamma\pm$ is the brine activity at molality, m, and
m_1 and m_2 represent the salinity contrast.

Yuan and Diederix[2] show that equation (2) can be expressed more simply as

$$\Delta U = \frac{C_e}{C_w + C_e} \Delta U_\infty \qquad (3)$$

where ΔU_∞ is the difference between the Nernst and liquid junction potentials for the salinity contrast used in equation (2). Equation (3) applies when the salinity contrast is small. Sen[11,12] has confirmed the validity of equation (3). Equation (3) becomes upon rearrangement:

$$C_e = C_w \cdot \frac{\Delta U}{\Delta U_\infty - \Delta U} \qquad (4)$$

Equation (4) shows that membrane potential measurements directly determine the clay conductivity.

2b. Induced Polarization Theory

In the Vinegar-Waxman[14] model for induced polarization of shaly sands, the phase angle, θ, is the ratio of quadrature conductivity, C_q, and rock conductivity, C_o, and is given as follows:

$$\theta = \frac{\lambda \cdot Q_v}{(C_w + C_e)\,\phi} \qquad (5)$$

where λ is the equivalent quadrature conductance,
ϕ is the porosity and
Q_v is the cation exchange capacity determined by conductometric titration.

Because the product of λ and Q_v is related to clay conductivity, it is anticipated that it is also influenced by clay geometry in the same manner as C_e. Clay geometry is incorporated by replacing Q_v with Q_{ve} to obtain:

$$\theta = \frac{\lambda \cdot Q_{ve}}{(C_w + C_e)\,\phi} \qquad (6)$$

By defining θ_∞ as follows:

$$\theta_\infty = \frac{\lambda \cdot Q_{ve}}{C_e \cdot \phi} \qquad (7)$$

equation (6) becomes

$$\theta = \frac{C_e}{C_w + C_e}\,\theta_\infty. \qquad (8)$$

Equation (8) casts the phase angle in terms of the clay conductivity directly instead of cation exchange capacity. Rearrangement of equation (8) yields

$$C_e = C_w \frac{\theta}{\theta_\infty - \theta} \qquad (9)$$

which shows that the phase angle θ also directly yields the clay conductivity when θ_∞ is known. Here θ_∞ can be seen to be a reference phase angle. Equation (9) exactly parallels the membrane potential equation for clay conductivity in equation (4), which leads to the following equality between shaly sand parameters

$$\frac{\theta}{\theta_\infty} = \frac{\Delta u}{\Delta u_\infty} \qquad (10)$$

The main difference is that Δu_∞ is calculated only from sodium transport properties while θ_∞ is a parameter that needs to be determined from additional clay conductivity measurements in equation (7) or (10). The reason for such similar theory is that both measurements involve the response of clay to local ionic gradients. For membrane potentials, these local ionic gradients are time independent, while for induced polarization, the local ionic gradients vary slowly in time[14].

Another quadrature conductivity model by Vinegar and Waxman uses λ_a where

$$\lambda_a = \frac{\lambda}{\phi} . \qquad (11)$$

The difference between the two models is the explicit porosity dependence when λ is used in equation (5). The determination of induced polarization parameters λ and λ_a require knowledge of the clay conductivity.

3. Experimental

3a. WS Group 2 Samples

Waxman and Smits[1] and Smits[13] performed conductivity and membrane potential measurements on the Group 2 samples at a number of different salinities. Smits used salinity contrasts of a factor of 2 which partitioned the salinity range from 6.144m to 0.012m, which is a factor greater than 500. Smits used arithmetic mean conductivities as a corresponding conductivity. This is in contrast to the "ideal" situation where the geometric mean salinity should be equal to C_w, which arises from the expression of membrane potential in equation (2). The difference between the arithmetic and geometric mean salinity is about 5 per cent.

Table 1 gives salinity contrasts that Smits used to measure membrane potentials, liquid junction and Nernst potentials for those ratios and corresponding conductivities and resistivities of arithmetic and geometric mean salinities. Salinity contrast is expressed in terms of molality, m, in moles/kg H_2O. Liquid junction potential values and Nernst potential values (Δu_∞) are calculated from sodium transport numbers and sodium chloride activity values at 25 degrees Celsius. It is preferable to use actual measured values for liquid junction in that any asymmetry potentials that may exist in the silver-silver chloride electrodes can be eliminated from the results.

Table 1

Salinity Contrasts, Corresponding Liquid Junction and Nernst Potentials and Average Brine Conductivities and Resistivities,

Salinity contrast $m_1:m_2$	liquid junction potential (mV)	Nernst potential (mV)	Arithmetic mean salinity		Geometric mean salinity	
			C_w (mmhos/cm)	R_w (ohm cms)	C_w (mmhos/cm)	R_w (ohm cms)
6.144 : 3.072	19.28	33.51	233.5	4.28	228.0	4.39
3.072 : 1.536	14.88	25.35	160.0	6.25	154.0	6.49
1.536 : 0.768	13.07	21.91	94.5	10.58	90.2	11.09
0.768 : 0.384	12.54	20.72	52.49	19.05	49.8	20.08
0.384 : 0.192	12.37	20.17	28.22	35.44	26.8	37.31
0.192 : 0.096	12.62	20.28	14.92	67.02	14.2	70.42
0.096 : 0.048	12.68	20.15	7.802	128.2	7.4	135.1
0.048 : 0.024	12.93	20.20	4.049	247.0	3.8	263.2
0.024 : 0.012	13.15	20.51	2.085	479.6	2.0	500.0

WS Group 2 samples originated from three different fields with a broad range of cation exchange capacity. The first seventeen of the 27 samples are Eocene age and contain mainly illite and kaolinite, 3 samples are Albion age and contain some montmorillonite in addition to kaolinite and illite and the remaining 7 samples, containing mainly montmorillonite, are Lower Tertiary in age.

The determination of clay conductivity requires accurate estimates of ΔU. WS Group 2 membrane potential values seem occasionally inconsistent. Decreasing salinity should result in increasing values of membrane potential for constant salinity ratio. In particular the membrane potentials for salinity contrast of 0.768m:0.384m and 0.024m:0.012m seem to be consistently low. This may have been caused by a systematic error in brine salinity or asymmetry potential in the silver-silver chloride electrodes. The results for 0.024m:0.012m are important because they represent the lowest salinity data. The results for salinity ratio of 0.768m:0.384m are less important because they correspond to a relatively high salinity.

3b. Bigfoot Samples

While the WS Group 2 samples provide abundant data, some uncertainties remain regarding the interpretation of the Group 2 data. The main uncertainties are as follows:

1) apparent systematic low membrane potential measurements at some salinity contrasts,
2) uncertain liquid junction potentials of group 2 samples which can cause significant scatter in clay conductivity and,
3) conductivity measurements were not made at the geometric mean salinity of the contrast used in membrane potential measurements.

It was decided that a set of simultaneous conductivity, membrane potential and subsequently induced polarization measurements may offer confirmation of the results of the WS Group 2 data set.

Four samples from Bigfoot Field, Frio County, Texas were selected. The clay type of the Bigfoot samples is predominantly montmorillonite and the samples are Cretaceous in age. Each sample was mounted in lucite for conductivity, membrane potential and induced polarization measurements which facilitated transfer of sample between measurements. The sample holders were very similar to those used by Vinegar-Waxman[14]. Details of the measurements and results are given in the Appendix. The salinity range used for the Bigfoot measurements duplicate those used for the most shaly of the group 2 samples, namely samples 25 - 27. Four of the Smits salinity contrasts were used which were those used for samples 25 and 27. Moreover these salinity contrasts were used to reconstruct Q_{ve} for the salinities (1.288m:.096m) used by Thomas[15] in his method for determining Q_v from membrane potential measurements.

4. Salinity Dependence of the Clay Conductivity, C_e

The clay conductivity is fundamental to shaly sand analysis. The essential role of membrane potential measurements is to directly determine the clay conductivity without any free parameters (equation (4)). In particular, clay conductivity is determined without knowledge of formation resistivity factor.

4a. WS Group 2 Samples

Table 2 contains clay conductivities for the WS Group 2 samples as a function of C_w (and R_w). The clay conductivity values are obtained as follows. Firstly the liquid junction potentials (Table 1) are subtracted from the membrane potential data of Smits to obtain ΔU values. These are combined with ΔU_∞ values at the appropriate salinity to determine clay conductivity, C_e, using equation (4). Note that clay conductivities determined at the two highest salinities may be affected by systematic errors in determination of membrane potential. Because shaly sand effects are generally unimportant at these salinities, discussion will be focussed on the salinity range from 94.5 mmho/cm and lower.

In addition to clay conductivity, an estimate of Q_{ve} is included[2] in Table 2. To examine the salinity dependence of the clay conductivity, it is better to normalize it with respect to Q_{ve}. The ratio of C_e/Q_{ve} is essentially a counterion conductance similar to the WS B value. Figure 1 shows C_e/Q_{ve} plotted against R_w (in ohm cms). Also shown in Figure 1 is a line representing the WS B value given as follows, where R_w is expressed in ohm cms:

$$B = 38.3.\ [1 - 0.8 * (-50/R_w)]\quad \text{mmho cm}^2/\text{mequiv} \qquad (12)$$

The Thomas method uses the B value to obtain Q_{ve}. Therefore, the plot of C_e/Q_{ve} should agree well with the B value in the salinity range where the Thomas salinities are used to determine Q_{ve}. At lower salinities, differences may arise because the salinity dependence of C_e is not exactly given by B from equation (12).

Table 2

WS Group 2 Clay Conductivity Values, C_e
(mmhos/cm)

Sample	C_w (mmhos/cm) / R_w (ohm cms)	233.50 / 4.28	160.00 / 6.25	94.50 / 10.58	52.49 / 19.05	28.22 / 35.44	14.92 / 67.02	7.80 / 128.20	4.05 / 247.00	2.09 / 479.60	Q_{ve}
1		4.40	0.00	1.89	0.54	0.67	0.36	0.33	0.32	0.20	0.02
2		5.13	0.13	3.26	2.08	2.02	1.66	1.27	1.02	0.57	0.06
3		-	0.57	4.19	1.46	1.66	1.06	1.07	0.84	0.71	0.05
4		-	-	3.72	3.11	3.33	2.37	2.01	1.36	0.69	0.09
5		-	2.70	5.62	4.16	3.97	3.02	2.73	2.28	1.87	0.12
6		6.59	3.02	6.11	3.63	4.42	3.31	3.06	2.00	1.63	0.13
7		6.59	4.68	6.45	5.36	4.85	3.99	3.32	2.86	2.26	0.15
8		5.86	5.35	5.14	4.57	4.05	3.20	2.76	2.43	1.82	0.12
9		5.86	2.70	6.60	4.04	4.99	3.20	3.48	2.81	2.13	0.13
10		-	8.09	11.79	8.41	9.63	7.49	6.45	5.76	1.56	0.28
11		-	8.09	10.18	10.16	8.94	6.77	5.49	2.92	1.91	0.26
12		8.82	14.60	15.57	15.06	15.43	12.34	11.54	10.72	6.61	0.45
13		-	14.60	17.54	16.26	15.97	13.36	12.80	10.99	8.82	0.42
14		9.58	12.38	15.17	14.60	14.13	11.98	12.28	9.73	8.30	0.43
15		15.77	19.55	24.63	23.04	21.71	16.27	13.94	9.07	4.68	0.64
16		-	29.27	38.39	39.45	40.03	35.93	35.51	32.48	11.62	1.16
17		-	27.52	35.07	34.80	36.17	31.28	33.25	22.01	19.09	1.04
18		15.77	24.11	28.89	28.31	29.63	25.97	26.15	25.82	30.31	0.86
19		13.41	18.44	27.44	20.80	20.68	17.97	18.27	16.72	17.18	0.64
20		10.33	13.85	18.77	17.09	16.46	14.46	13.36	12.86	16.35	0.51
21		-	-	16.94	14.81	14.13	13.10	13.36	7.74	11.62	0.45
22		23.97	-	52.55	50.50	49.33	45.60	44.95	52.78	39.84	1.46
23		28.28	-	77.47	59.98	60.17	57.12	85.78	83.01	80.15	1.74
24		32.73	-	70.09	70.68	72.70	64.71	78.11	49.09	131.60	2.04
25		43.09	-	95.80	103.80	116.30	101.50	-	-	-	2.98
26		45.05	-	102.10	112.80	120.00	116.60	144.80	93.37	99.73	3.19
27		42.11	-	102.10	110.80	132.60	119.60	-	-	-	3.25

1991 SCA Conference Paper Number 9115

The first 17 samples, shown as circles, contain no montmorillonite and the clay conductivity generally decreases as a function of decreasing salinity, which is in accord with the WS B value. On the other hand samples 18-27, shown as solid triangles, are samples containing montmorillonite and show less systematic decrease in clay conductivity. Clearly samples 19 and 21 show systematic decrease with salinity in Table 2. However, samples 25-27 tend to show that the clay conductivity initially increases with decreasing salinity.

4b. Bigfoot Samples

Table 3 contains clay conductivities as a function of C_w for Bigfoot samples and are shown in Figure 1 as open triangles. The salinity dependence of the clay conductivity is not clear but the behavior here is similar in character to samples 25-27. It is unclear whether the clay conductivity increases or decreases consistently. The clay conductivity shows an increase in value at 14.1 mmhos/cm.

Table 3

Bigfoot Clay Conductivity Values, C_e (mmhos/cm)

	C_w (mmhos/cm)				
	90.09	49.31	26.72	14.1	Q_{ve}
Sample					
1	50.3	52.2	43.6	55.0	1.56
2	50.2	48.7	41.9	54.3	1.50
3	45.5	50.3	43.3	53.5	1.49
4	45.6	52.0	43.6	61.6	1.54

Clay conductivity variations in Tables 2 and 3 can be interpreted as changes in clay geometry that may take place as salinity is varied. This can happen with montmorillonite-bearing samples because montmorillonite is known to swell when the salinity of equilibrating brine is decreased[16]. Accordingly, the unusual clay conductivity variations of Group 2 samples 18-27 and the Bigfoot samples may be attributed to changes in montmorillonite morphology as salinity is reduced.

4c. Effective Cation Exchange Capacity, Q_{ve}

Yuan and Diederix[2] introduced the idea of effective exchange capacity, Q_{ve}, which was obtained from the membrane potential method of determining exchange capacity introduced by Thomas[15]. It was found that the values of Q_{ve} were often different from Q_v values for the Group 2 samples, which are attributed to clay geometry[2,3]. The concept of Q_{ve} is now expanded.

The necessity of determining Q_{ve} arises from the partition of the clay conductivity into two factors; the equivalent counterion conductivity, B, and the effective exchange capacity, Q_{ve}. However because the clay conductivity is fixed by membrane potential measurements, Q_{ve} can be defined by the ratio of C_e/B where B may be given by equation (12). The ratio, C_e/B, may be slightly different from the Thomas value of Q_{ve} and to differentiate Q_{ve} values we refer to the ratio of C_e/B as $Q_{ve}(C_w)$ to denote possible salinity dependence.

$Q_{ve}(C_w)$ may be salinity dependent if the clay conductivity salinity dependence is not exactly cancelled by the salinity dependence of B. $Q_{ve}(C_w)$ can be calculated for each clay conductivity value at each salinity in Tables 2 and 3 and so arise at a salinity dependence of $Q_{ve}(C_w)$. However, a different expression of B will yield a different salinity dependence of $Q_{ve}(C_w)$.

In tables 2 and 3, Q_{ve} and not $Q_{ve}(C_w)$ values are included. These values were determined by the method proposed by Yuan and Diederix[2] for obtaining Q_{ve} from a number of membrane potential measurements made over smaller salinity contrasts. The value for Q_{ve} for sample 1 is included although, as noted earlier[2], there was some epoxy penetration into the sample rendering the conductivity data questionable. On the other hand, sample 1 membrane potential data is valid because membrane potential measurements are not dependent on sample shape.

5. Salinity Dependence of F*

A brief discussion of the salinity dependence of F* is given here and more detailed discussion of the salinity dependence of F* is given elsewhere[17].

5a. WS Group 2 Samples

The clay conductivity data from Table 4 is combined with C_o-C_w data to calculate F* using equation (1). Table 4 shows these values as a function of C_w and compares them with the usual method of calculating F* from high salinity C_o-C_w data, referred to as the multiple salinity method, F^*_{ms}. F^*_{ms} was calculated from a linear regression through at least 4 high salinity data points. If sufficient points allowed, only C_o values were used where C_w was greater than 50 mmhos/cm. The high salinity F* values agree well with F^*_{ms}.

For WS samples 1 through 9, F* is essentially constant. It appears from this data that the WS assumption of constant F* is very reasonable and the WS model correctly describes the salinity dependence of the clay conductivity. It is quite remarkable how well the assumption of constant F* works for these shaly sands.

Samples 10-17 show more variable behavior. For example, sample 11 shows a steady decrease of F* with salinity simultaneously with a steady decrease of clay conductivity with salinity. This may be due to the rather sharp decrease in clay conductivity in going from 7.802 mmhos/cm to 4.049 mmhos/cm. On the other hand, sample 14 shows a modest increase in F* even though the clay conductivity shows no abnormality. Similarly for sample 16, with the exception of the lowest salinity data point which is considered spuriously low, the clay conductivity shows a steady decrease and F* shows steady increase with decreasing salinity. These samples are discussed in detail elsewhere[17].

For montmorillonite-bearing samples (18-27) F* shows clear salinity dependence. For the more shaly samples, F* increases at least 50% over the salinity range.

The key to whether F* varies appears to lie in the relative magnitude of C_e to C_w. For samples 1-9, C_e values remain smaller than C_w and F* is essentially constant for these samples. Samples 10-17 have higher clay conductivity than brine conductivity. The changes in F* for these samples are fairly modest and the WS model would work well enough in providing reasonable clay conductivity values. On the other hand, samples 18-27 contain values of clay conductivity that are significantly greater than brine conductivity.

Table 4

WS Group 2 Formation Resistivity Factors

Sample	C_w (mmhos/cm) / R_w (ohm cms)	233.50 / 4.28	160.00 / 6.25	94.50 / 10.58	52.49 / 19.05	28.22 / 35.44	14.92 / 67.02	7.80 / 128.20	4.05 / 247.00	2.09 / 479.60	F^*_{ms}
1		12.46	12.12	12.28	11.97	11.84	11.92	11.96	12.05	11.86	12.33
2		14.38	14.03	14.29	14.10	14.13	14.18	14.10	14.05	12.95	14.23
3		-	11.19	11.49	11.10	11.15	11.02	11.26	11.25	11.59	11.30
4		-	-	48.87	48.78	49.07	47.06	47.61	45.12	39.61	48.47
5		-	14.78	15.15	14.91	14.91	14.71	14.82	14.72	14.76	14.90
6		18.91	18.63	19.09	18.52	19.06	18.77	19.11	18.32	17.91	18.73
7		27.16	26.82	27.07	27.03	27.29	27.00	26.91	27.38	27.18	27.05
8		25.96	25.80	25.61	25.59	25.65	25.33	25.52	26.18	25.76	25.93
9		18.27	18.02	18.58	18.00	18.55	17.68	18.75	18.53	18.01	18.18
10		-	158.60	158.40	151.50	158.40	153.60	154.30	164.10	93.30	163.20
11		-	173.80	176.80	179.00	176.10	171.50	166.50	142.20	123.60	174.30
12		43.82	45.35	45.79	46.27	48.77	47.51	53.48	60.02	43.61	44.61
13		-	45.95	46.88	46.45	47.72	46.96	49.59	52.09	48.57	45.97
14		32.32	32.59	33.03	33.55	34.35	33.77	36.81	36.25	35.31	32.87
15		-	154.80	157.80	157.70	160.10	152.00	153.60	138.30	98.50	158.80
16		-	62.88	68.45	70.72	76.26	77.33	85.76	96.44	42.50	65.21
17		-	44.75	47.64	47.96	51.51	50.07	60.15	47.13	44.76	45.02
18		17.93	18.67	19.31	19.66	21.16	21.25	25.10	27.91	34.43	18.53
19		16.80	17.09	18.45	17.75	18.62	18.84	21.06	23.21	26.98	17.13
20		12.97	13.17	13.68	13.67	14.09	14.25	15.06	16.64	24.12	13.20
21		-	-	16.01	16.14	16.61	17.83	22.11	16.75	24.54	14.85
22		33.97	-	39.85	40.87	43.32	44.79	48.31	59.67	46.81	35.75
23		25.27	-	33.01	30.98	33.86	36.76	59.38	64.20	64.65	26.92
24		41.86	-	50.33	52.64	57.02	57.70	77.96	53.39	137.70	44.93
25		50.66	-	64.08	69.76	65.68	78.58	-	-	-	56.12
26		37.14	-	47.61	52.64	59.77	64.30	83.59	61.00	67.74	41.49
27		39.15	-	50.68	54.98	66.72	65.97	-	-	-	44.36

F* variation is represented by plotting normalized values, F^*/F^*_{ms}, against C_e/C_w, which is shown in Figure 2. Samples without montmorillonite are shown as circles while those with montmorillonite are shown as triangles.

5b. Bigfoot Samples

Bigfoot F* and corresponding F^*_{ms} values are shown in Table 5 and are plotted in Figure 2 as open triangles. The Bigfoot data are consistent with the Group 2 samples data and represent confirmation that F* can be salinity dependent.

Table 5

Bigfoot Formation Resistivity Factors, F*

	C_w (mmhos/cm)				
	90.09	49.31	26.72	14.1	F^*_{ms}
Sample					
1	27.9	30.6	30.6	38.4	24.9
2	23.2	24.4	25.5	32.7	20.4
3	22.0	23.8	25.5	32.7	19.7
4	21.7	24.2	24.4	33.2	20.6

Moreover, the Bigfoot data remove two uncertainties of the Group 2 data. Firstly, measuring conductivities at arithmetic mean salinities as opposed to geometric mean salinities is not important. This is due to the fact that the clay conductivity is slowly varying with salinity. A small change in salinity does not greatly affect the clay conductivity. Secondly, the simultaneous measurement of liquid junction potential may not have reduced the scatter in clay conductivity values. Doing so did not eliminate clay conductivity scatter for the Bigfoot samples.

6. Salinity Dependence of m*

6a. WS Group 2 Samples

In engineering situations, the shaly sand lithologic exponent, m*, defined by:

$$F^* = \phi^{-m^*} \qquad (13)$$

is a parameter that is used for interpreting resistivity logs. The fact that F* may be salinity dependent implies that either m* or ϕ may be salinity dependent. While no measurable change in bulk dimensions occurred, it is possible that clay morphology, in particular for montmorillonite, may have changed with decreasing salinity so that a change in porosity has occurred. Consequently, a change in F* most likely implies a change in both porosity and m*. However, it is assumed for the calculations below that no change in porosity has occurred and therefore changes in F* imply changes in m*.

Table 6

WS Group 2 m* Values

Sample	C_w (mmhos/cm)	233.50	160.00	94.50	52.49	28.22	14.92	7.80	4.05	2.09	
	R_w (ohm cms)	4.28	6.25	10.58	19.05	35.44	67.02	128.20	247.00	479.60	m^*_{ms}
1		1.76	1.74	1.75	1.73	1.73	1.73	1.73	1.74	1.73	1.76
2		1.72	1.70	1.72	1.71	1.71	1.71	1.71	1.70	1.65	1.71
3		-	1.65	1.67	1.64	1.65	1.64	1.65	1.65	1.67	1.66
4		-	-	1.54	1.54	1.54	1.53	1.53	1.51	1.46	1.54
5		-	1.44	1.45	1.44	1.44	1.44	1.44	1.44	1.44	1.44
6		1.91	1.90	1.92	1.90	1.92	1.91	1.92	1.89	1.87	1.91
7		1.87	1.86	1.87	1.87	1.87	1.87	1.86	1.87	1.87	1.87
8		1.84	1.84	1.84	1.84	1.84	1.83	1.83	1.85	1.84	1.84
9		1.80	1.79	1.81	1.79	1.81	1.78	1.82	1.81	1.79	1.80
10		-	2.44	2.44	2.41	2.44	2.42	2.42	2.45	2.18	2.45
11		-	2.48	2.49	2.50	2.49	2.47	2.46	2.38	2.32	2.48
12		1.71	1.73	1.73	1.74	1.76	1.75	1.80	1.86	1.71	1.72
13		-	1.73	1.74	1.74	1.75	1.74	1.77	1.79	1.76	1.73
14		1.58	1.58	1.59	1.59	1.60	1.60	1.63	1.63	1.62	1.58
15		-	2.11	2.12	2.12	2.13	2.11	2.11	2.07	1.92	2.12
16		-	1.82	1.86	1.87	1.91	1.91	1.96	2.01	1.65	1.84
17		-	1.93	1.97	1.97	2.01	1.99	2.08	1.96	1.93	1.94
18		2.14	2.17	2.19	2.21	2.26	2.26	2.39	2.46	2.62	2.16
19		2.09	2.10	2.16	2.13	2.17	2.17	2.26	2.33	2.44	2.10
20		1.90	1.91	1.94	1.94	1.96	1.97	2.01	2.08	2.36	1.91
21		-	-	1.93	1.94	1.96	2.01	2.16	1.96	2.23	1.88
22		2.36	-	2.47	2.49	2.53	2.55	2.60	2.74	2.58	2.40
23		2.28	-	2.47	2.42	2.48	2.54	2.88	2.93	2.94	2.32
24		2.44	-	2.56	2.59	2.64	2.65	2.84	2.60	3.21	2.48
25		2.34	-	2.48	2.53	2.50	2.60	-	-	-	2.40
26		2.45	-	2.62	2.69	2.78	2.83	3.00	2.79	2.86	2.53
27		2.34	-	2.51	2.56	2.68	2.68	-	-	-	2.42

The values for m* using equation (12) are given in Table 6 showing m* as a function of salinity (for constant porosity). The value of m* from the multiple salinity technique is included for comparison and referred to as m^*_{ms} (obtained from F^*_{ms} using equation (13)).

Again for samples 1-9, m* remains constant. Modest changes in m* occur for samples 10-17 while more significant changes in m* occur for samples 18-27.

6b. Bigfoot Samples

Table 7 contains values for m* from equation (13) as well as m^*_{ms} values from the multiple salinity technique. The changes in m* for the Bigfoot samples are essentially the same as the changes in m* for the shaliest samples of the Group 2 samples.

Table 7

Bigfoot m* Values

	C_w (mmhos/cm)				
	90.09	49.31	26.72	14.1	m^*_{ms}
Sample					
1	2.43	2.50	2.50	2.66	2.35
2	2.47	2.51	2.54	2.74	2.37
3	2.43	2.49	2.54	2.74	2.34
4	2.29	2.37	2.38	2.61	2.25

7. Salinity Dependence of λ

The equivalent quadrature conductance, λ, was calculated for Bigfoot samples using equation (6) while λ_a was obtained using equations (6) and (10) as follows:

$$\lambda = \theta \cdot (C_w + C_e) \cdot \phi / Q_{ve} \qquad (14)$$

$$\lambda_a = \theta \cdot (C_w + C_e) / Q_{ve} \qquad (15)$$

Results for λ and λ_a for Bigfoot samples are given in Tables 8a and 8b. These results are obtained using $Q_{ve}(C_w)$ determined at each salinity as opposed to Q_{ve}. Thus, any clay geometric effect from salinity dependence is captured in Q_{ve} and not in λ or λ_a. This is equivalent to using C_e/B in place of Q_{ve} and therefore the Bigfoot data actually determines the ratio λ/B or λ_a/B. The determination of λ or λ_a is completed by using a value of B from equation (12) at the appropriate salinity.

Table 8a

Bigfoot λ Values

	C_w (mmhos/cm) 49.31	26.72	14.1	ϕ(%)
Sample				
1	0.104	0.113	0.089	25.4
2	0.113	0.12	0.087	28.0
3	0.119	0.125	0.092	28.0
4	0.105	0.116	0.078	26.1

Table 8b

Bigfoot λ_a Values

	C_w (mmhos/cm) 49.31	26.72	14.1	ϕ(%)
Sample				
1	0.411	0.427	0.351	25.4
2	0.403	0.427	0.311	28.0
3	0.424	0.446	0.328	28.0
4	0.402	0.444	0.299	26.1

Table 9 contains average λ and λ_a values as well as standard deviations about the mean for the four samples. In addition values for the parameter θ_∞ as a function of salinity are included. Comparison of the average λ values with the Vinegar-Waxman results is shown in Figure 3. The agreement between average λ and Vinegar-Waxman data is excellent. The results from Table 9 imply that λ has a lower standard deviation and therefore may be the preferrable model. However, more experiments over a wider range of porosity and salinity are needed before it is clear whether λ or λ_a is the better model.

θ_∞ is defined by equation (7), and is equivalent to the ratio of $\lambda/(B\phi)$. For λ_a, θ_∞ would be defined without the factor of ϕ in the denominator. Accordingly, θ_∞ is generally independent (to within a factor of porosity) of the sample of interest and is the parameter needed to convert phase angle to clay conductivity.

Table 9

Mean and Standard Deviations for λ and λ_a, Average Reference Phase Angle, θ_∞ Bigfoot Samples

	C_w (mmhos/cm)		
	49.31	26.72	14.1
average λ	0.11	0.118	0.087
standard deviation	0.007	0.005	0.006
average λ_a	0.41	0.441	0.322
standard deviation	0.01	0.009	0.023
θ_∞	0.0115	0.0146	0.0139

8. Discussion

The focus of this paper has been the application of membrane potential measurements to the determination of shaly sand parameters. Because membrane potential measurements directly determine clay conductivity, the salinity dependence of any shaly sand parameters begins with incorporating whatever salinity dependence clay conductivity values have. Accordingly, the shaly sand formation resistivity factor, Archies lithologic exponent, induced polarization parameters, and effective cation exchange capacity may each be salinity dependent.

This approach is in contrast with the WS approach of assuming F* constant. Moreover in the WS approach characterization of the clay conductivity relies on the cation exchange capacity, Q_v. However, it has been demonstrated[3] that Q_v is a relatively poor characterization of clay conductivity and accordingly any shaly sand model[4,7,9] that relies upon Q_v is likely to improperly account for the behavior of shaly sand parameters. Improvements in shaly sand description come from casting shaly sand equations in terms of Q_{ve} or C_e directly.

Several features of the clay conductivity have been observed from the Group 2 and Bigfoot samples:

1) clay type appears to have an effect on the overall behavior of the clay conductivity.

2) for kaolinite-illite clays, the clay conductivity decreases smoothly as salinity decreases. The salinity dependence follows essentially that proposed by WS and Smits in the formulation of the equivalent counterion conductance.

3) for montmorillonite clays the clay conductivity appears to increase as salinity decreases when the clay conductivity is much greater than the brine conductivity.

Consequently, it appears that the clay conductivity may not be described by a universal clay counterion conductance. For kaolinite-illite-bearing shaly sands the WS formulation appears adequate, but for montmorillonite-bearing shaly sands some other form may be necessary. Perhaps a reliable strategy is to measure the clay conductivity for the sample at the salinity of interest because membrane potentials are relatively expedient measurements. However the dependence of clay conductivity on other parameters such as temperature and cation-type need to be further explored for montmorillonite-bearing samples at low salinity. The behavior of kaolinite-illite-bearing samples at very low salinity where C_e is less than C_w also needs further investigation.

The salinity dependence of the formation resistivity factor has greater implications. Firstly, for situations where the clay conductivity is less than the brine conductivity, the WS assumption of constant F* is very good. When the clay conductivity is large compared with the brine conductivity, it is possible that the conductive pathways of the clays are different from the brine conductive pathways at high salinity. The non-linearity of the C_o-C_w plot is indicative of this and has been pointed out by others[11,12]. The essential feature is the behavior of the clay conductivity at low salinities. It is essential that the behavior of the clay conductivity be better understood before the proper functionality of the formation factor is known. It may be possible that F* approaches an asymptotic value at low salinities or steadily increases with decreasing salinity or F* gets smaller at asymptotically low salinities.

Induced polarization results have been very consistent with the Vinegar-Waxman results. Results for λ were in excellent agreement with values obtained by Vinegar and Waxman. The data set is too small to determine whether λ or λ_a is the better induced polarization model although λ values have lower scatter and better agreement with Vinegar-Waxman data. An improvement in the theory of quadrature conductance is to cast it in terms of C_e instead of Q_v (equation (8)). This reduces ambiguity by eliminating the need to determine Q_v and relates the phase angle to the clay conductivity directly.

The present paper has focussed only on shaly samples saturated with NaCl brines. Membrane potential measurements can also be used to study the dependence of the clay conductivity on temperature, cation type and partial brine saturation[18].

9. Conclusions

- Measurements entailing simultaneous conductivity, electrokinetic and induced polarization measurements are necessary for the proper determination of shaly sand parameters.

- Membrane potential measurements directly determine the clay conductivity as a function of salinity.

- For the WS Group 2 data set, samples containing kaolinite and illite have clay conductivities that gradually decrease with decreasing salinity. The WS model works well for these samples.

- For the WS Group 2 data set, samples with montmorillonite have clay conductivity that appear to increase with decreasing salinity.

- New data on a set of montmorillonite bearing shaly sands is very consistent with results from the WS Group 2 samples.

- The effective cation exchange capacity, $Q_{ve}(C_w)$, defined as the ratio of clay conductivity to equivalent counterion exchange capacity, (C_e/B), may be salinity dependent depending on the relative salinity dependence of C_e and B.

- The Yuan-Diederix equation for brine saturated shaly sands contains a single parameter namely the formation resistivity factor. Data from the WS Group 2 and new shaly sand data both show that the shaly sand formation resistivity factor may be salinity dependent.

- At high salinities, F* from membrane potential measurements agrees very well with F* obtained from the high salinity C_o-C_w data, referred to as F^*_{ms}.

- Salinity dependence of the shaly sand formation resistivity factor arises when the clay conductivity is much larger than the brine conductivity. Salinity dependence of F* is greatest for montmorillonite-bearing shaly sands where the clay conductivity is generally large but may also be due to changes in montmorillonite structure as salinity is reduced.

- The reason for salinity dependence of F* is the conductive pathways, when brine conductivity is dominant, are different from the conductive pathways, when clay conductivity is dominant.

- The implication of salinity-dependent F* is that conductivity and membrane potential measurements are necessary for the proper determination of shaly sand parameters when the clay conductivity is greater than the brine conductivity.

- The shaly sand lithology exponent, m*, becomes salinity dependent when F* becomes salinity dependent.

- Salinity dependence of shaly sand parameters $Q_{ve}(C_w)$, F* and m* has been introduced. Each parameter already has a salinity independent interpretation Q_{ve}, F^*_{ms} and m^*_{ms} determined from measurements over a wider salinity range.

- The salinity dependence of induced polarization parameters, λ and λ_a, agree very well with Vinegar-Waxman estimates. From this limited data set λ appears to be a better description for induced polarization of shaly sands due to lower scatter and better agreement with Vinegar-Waxman data. However, the data set is too small to confidently decide between λ and λ_a.

- A new induced polarization equation has been suggested where the quadrature conductance is directly proportional to clay conductivity instead of cation exchange capacity. The new equation exactly parallels the membrane potential equation for clay conductivity.

- More study is required to delineate the salinity dependence of shaly sand parameters, especially the clay conductivity, when the clay conductivity greatly exceeds the brine conductivity.

10. Acknowledgments

The author acknowledges the assistance of Bobby Shannnon who made conductivity, membrane potential and phase angle measurements on Bigfoot samples. The author also benefitted from many discussions with researchers at both Koninklijke/Shell Exploratie en Produktie Laboratorium, Rijswijk, The Netherlands and Bellaire Research Center, Houston, Texas. He thanks the management at Shell Development Company for permission to publish this work.

11. References

1. Waxman, M.H. and Smits, L.J.M., (1968) Electrical Conductivities in Oil-Bearing Shaly Sands, Transactions, AIME, v243, part II, 107-122.

2. Yuan, H.H. and Diederix, K.M.,(1989) The Role of Membrane Potential Measurements in Shaly Sand Evaluation, Log Analyst, vol 30, 415-423.

3. de Waal, J.A., (1987) The Influence of Clay Distribution on Shaly Sand Conductivity, SPE 16786, paper presented at the 62nd Annual Fall Technical Conference and Exhibit, Dallas, September 27-30.

4. Worthington, P.F. (1985) The Evolution of Shaly Sand Concepts in Reservoir Evaluation, The Log Analyst, vol 26, pp 23-40.

5. Steward, H.E., and Burck, L.J.S., (1986) Improved Cation Exchange Capacity/Q_v Determination using the Multi-temperature membrane potential test, The Log Analyst, vol 27, p25.

6. Silva, P.L., and Bassiouni, Z., (1987) Prediction of Membrane Potentials in Shales and Shaly Sands Using the S-B Conductivity Model, The Log Analyst, vol 28, pp 129-137.

7. Clavier, C., Coates, G., and Dumanoir, J., (1977), The Theoretical and Experimental Bases for the 'Dual Water' Model for the Interpretation of Shaly Sands, SPE 6859, paper presented at the 52nd Annual Fall Technical Conference and Exhibition of the SPE, Denver, October 9-12.

8. Cohen, R.R., and Radke, C.J., (1987) A Patchy Charge Model for the Surface Conductivity of Clays, SPE 15968, paper presented at the SPE International Symposium on Oilfield Chemistry, San Antonio, February 4-6.

9. Stenson, J.D. and Sharma, M.M., (1989) A Petrophysical Model of Shaly Sands, SPE 19574, paper presented at the 64th Annual Fall Technical Conference and Exhibit, San Antonio, October 8-11.

10. Hardwick, A., (1989), Xls, A New Shale Parameter for Resistivity Log Evaluation, SPE 19576, paper presented at the 64th Annual Fall Technical Conference and Exhibit, San Antonio, October 8-11.

11. Sen, P.N., (1989) The Influence of Microgeometry on Membrane Potential of Shaly Sands, Geophysics, vol 54, pp 1543-1553.

12. Sen, P.N., (1990) Model-Independent Relationship between Conductivity and Membrane Potential of Shaly Sands, paper presented at the 13th European Formation Evaluation Symposium, Budapest, Hungary, October 22-26.

13. Smits, L.J.M. (1968), S.P. Log Interpretation in Shaly Sands, Soc. Pet. J., June, pp. 123-136.

14. Vinegar, H.J. and Waxman, M.H., (1984) Induced Polarization of Shaly Sands, Geophysics, vol 49, pp 1267-1287.

15. Thomas, E.C. (1976), The Determination of Q_v from Membrane Potential Measurements on Shaly Sands, Transactions, AIME, v.261, Part I, 1087-1096.

16. van Olphen, H., An Introduction to Clay Colloid Chemistry, John Wiley and Sons, Inc, New York, 1977

17. Yuan, H.H. (1991), Salinity Dependence of the Formation Resistivity Factor, SPE 22665, paper to be presented at the SPE 66th Annual Fall Technical Conference and Exhibit, Dallas, October.

18. Yuan, H.H. unpublished

12. Nomenclature

B	equivalent counterion conductance factor (mho cm^2/eq)
C_e	specific conductivity of clay counterions (mho/cm)
C_o	specific conductivity of brine saturated rock (mho/cm)
C_q	specific quadrature conductivity of brine saturated rock (mho/cm)
C_w	brine specific conductivity (mho/cm)
E_m	measured membrane potential (mV)
E_t	liquid junction potential (mV)
F^*	shaly sand formation resistivity factor
F^*_{ms}	shaly sand formation resistivity factor obtained from linear regression of high salinity C_o-C_w data
Q_v	concentration of exchange counterions (meq/ml) determined from CEC using conductometric titration on crushed sample
Q_{ve}	concentration of exchange counterions (meq/ml) determined using the Thomas membrane potential method (salinity contrast 1.288m:0.096m) of determining exchange capacity. Value includes effects of clay geometry and is often different from Q_v
$Q_{ve}(C_w)$	concentration of exchange counterions (meq/ml) determined from ratio of clay conductivity from membrane potential measurements and equivalent counterion conductance.
R_w	brine resistivity (ohm cm)
m^*	shaly sand lithology exponent obtained from F^*
m^*_{ms}	shaly sand lithology exponent obtained from F^*_{ms}
ΔU	difference between membrane potential and liquid junction potential (mV)
ΔU_∞	ΔU for perfect membrane (mV)

λ equivalent quadrature conductivity (mho cm^2/eq) defined in equation (7) and (17)

λ_a equivalent quadrature conductivity (mho cm^2/eq) defined in equation (18)

$m\gamma\pm$ brine activity at molality, m

m_1, m_2 molal salinity contrast.

ϕ porosity - pore volume/bulk volume

θ phase angle - ratio of C_q/C_o

θ_∞ reference phase angle defined in equation (7) and equal to $\lambda/(B\phi)$

t_{Na} sodium Hittorf transport number

Appendix

Experimental Details and Results for Bigfoot Samples

Petrophysical data for Bigfoot samples are given in Table A1.

Table A1

Petrophysical Data for Bigfoot Samples

Sample	Grain Density (grams/cc)	Porosity (%)	Permeability (mD)
1	2.705	25.4	10.3
2	2.681	28.0	8.4
3	2.691	28.0	9.0
4	2.687	26.1	4.3

Conductivity measurements were made at 6 different salinities ranging from 233.6 mmhos/cm to 14.1 mmhos/cm. Measurements were made in the two electrode configuration using an ESI model 253 conductivity bridge. A blank conductivity was subtracted to obtain the proper sample conductivity. The samples were flushed repeatedly until stable conductivity values were obtained. This often took more than a week and sometimes more than 2 weeks. After a stable conductivity reading was obtained, the sample was placed in a membrane potential apparatus with a salinity contrast of a ratio of 2 for which ΔU_∞ was known (Smits salinities) and for which the geometric mean salinity conductivity was equal to the conductivity of the brine used for the conductivity measurement. The exception to this were the highest two salinities where no membrane potential measurements were made due to water transport effects that cause membrane potential measurements to be underestimated. Conductivity results are given in Table A2. Relative errors are on the order of 1 per cent. Conductivity values were corrected to 23 degrees centrigrade.

Table A2

Conductivity of Bigfoot Samples, C_o (mmhos/cm)

Sample	1	2	3	4
C_w (mmhos/cm)				
233.6	10.78	13.11	12.93	13.19
159.0	7.86	9.43	9.42	9.46
90.09	5.03	6.06	6.16	6.24
49.31	3.32	4.01	4.19	4.18
26.76	2.30	2.69	2.75	2.88
14.1	1.8	2.09	2.07	2.28

EMF readings were taken using a Kiethly 519 electrometer. Liquid junction potentials were made after each measurement and subtracted from the measured EMF reading to obtain ΔU values. This is in contrast with subtracting the ideal liquid junction potentials for the Group 2 samples. Membrane potentials were performed at 4 different salinities, where the geometric conductivities ranges from 90.09 mmhos/cm to 14.1 mmhos/cm. Membrane potentials are given in Table A3. Relative errors are on the order of 1 per cent but up to 3 per cent for the higher potentials. This is because the membrane potentials are beginning to approach the Nernst potential.

Table A3

Membrane Potential of Bigfoot Samples, ΔU (mV)

Sample #	1	2	3	4
C_w (mmhos/cm)				
90.09	7.85	7.84	7.35	7.36
49.31	10.65	10.29	10.46	10.63
26.76	12.50	12.31	12.47	12.50
14.1	16.14	16.10	16.05	16.50

Quadrature conductivity measurements expressed in terms of phase angle were made at three salinities using an HP4192 Impedance Analyzer. Brine conductivities ranged from 49.31 mmhos/cm to 14.1 mmhos/cm. Due to instrument performance, measurements were made in the 500 - 1000 Hz range. A blank measurement of the brine was subtracted from the measured quadrature conductivity. Blank values were typically 0-2 milliradians. Phase angle measurements are given in Table A4. Absolute error in phase angle measurements is 0.2 milliradians.

Table A4

Phase Angle of Bigfoot Samples, θ (milliradians)

Sample #	1	2	3	4
C_w (mmhos/cm)				
49.31	5.9	5.6	6.0	5.8
26.76	9.1	8.6	9.1	9.1
14.1	12.1	10.7	11.2	10.5

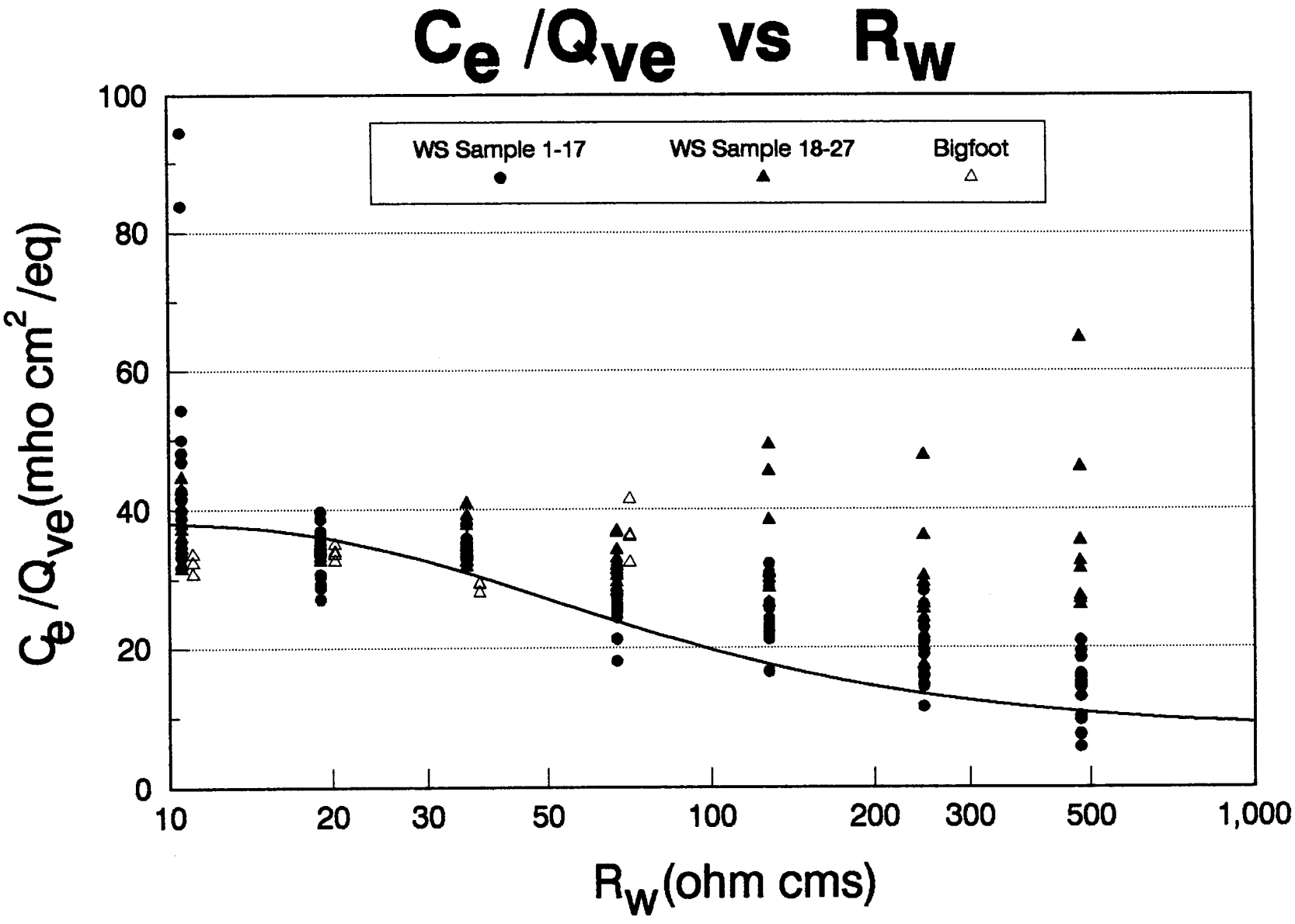

Figure 1. Salinity Dependence of the Clay Conductivity.

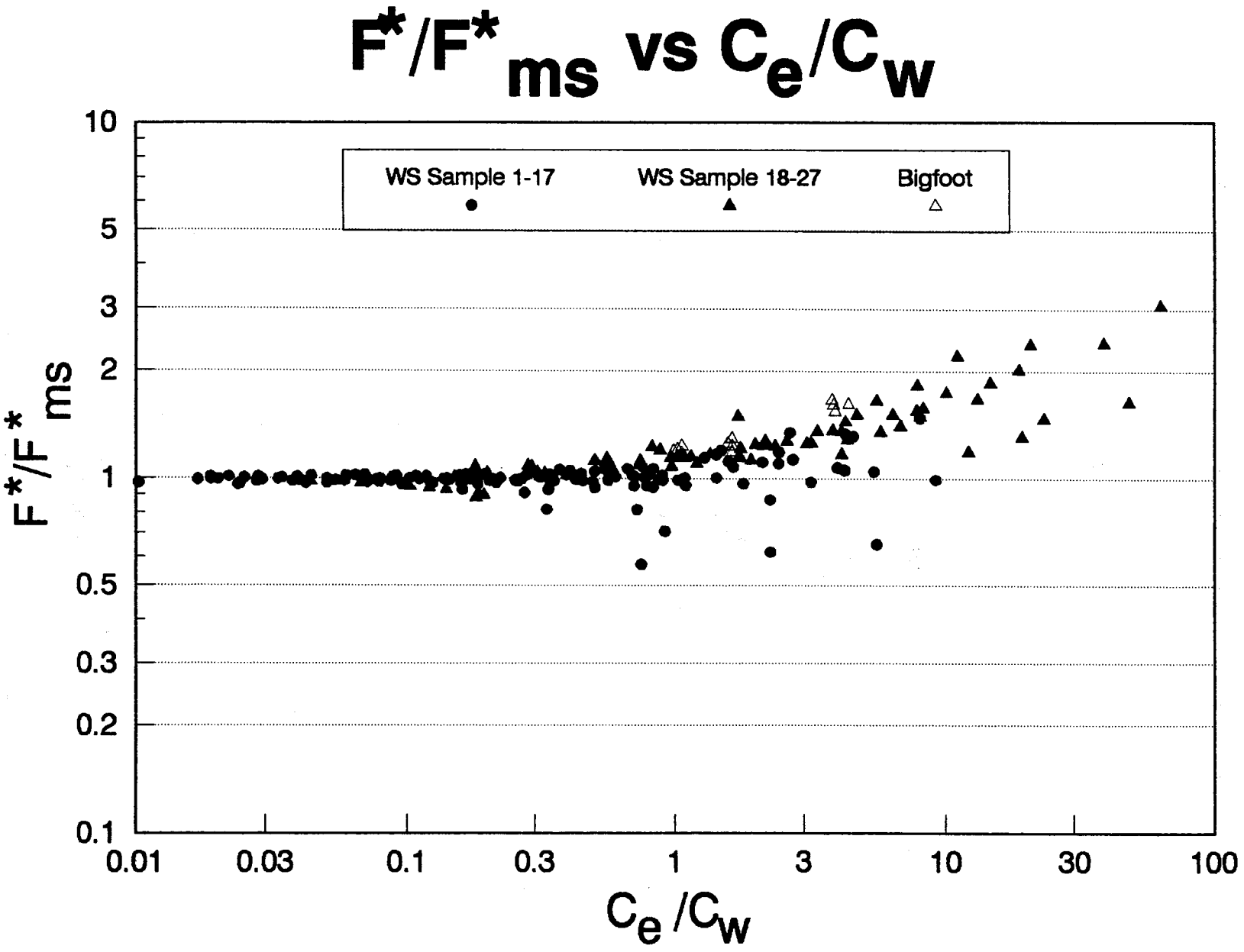

Figure 2. Salinity Dependence of the Shaly Sand Formation Resistivity Factor.

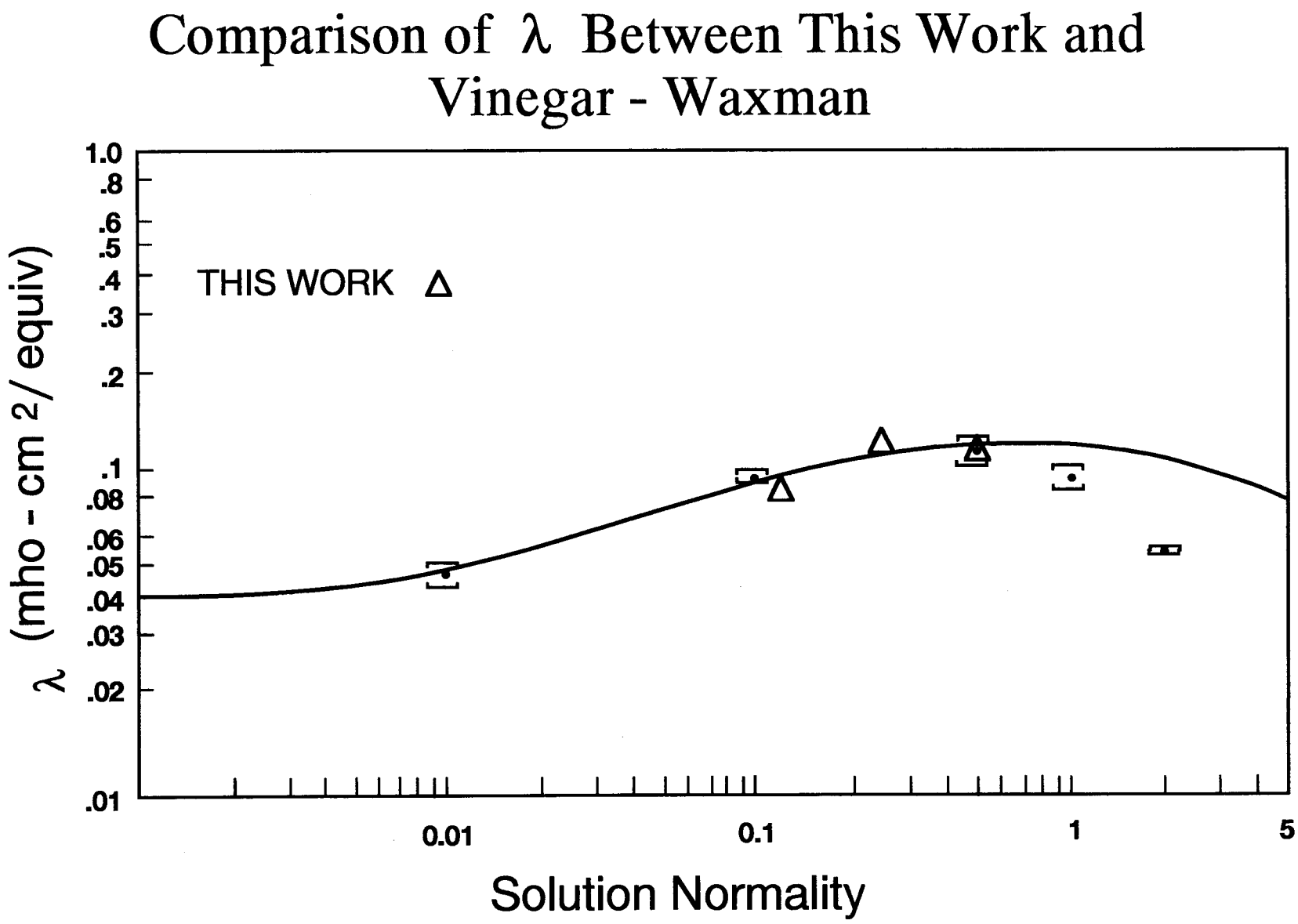

Figure 3. Comparison of Equivalent Quadrature Conductance Values.

OBSERVATIONS OF ROCK FABRIC CONTROLS ON THE ELECTRICAL PROPERTIES OF SANDSTONES

by Gerald A. LaTorraca
Connie G. Hall

ABSTRACT

We report electrical properties measurements on 323 sandstone samples with minimal amounts of predominantly authigenic clays. All measurements were made at Chevron during the past 15 years using net effective reservoir pressure and room temperature. Almost all of the samples are fairly well consolidated. The most common clay is kaolinite with lesser amounts of illite, chlorite, glauconite, and traces of smectite. Our objectives in this paper are to document the ranges of the cementation (**m**) and saturation (**n**) exponents in our data and to relate the values of **m** and **n** to rock fabric.

We "clay corrected" the measured values of resistivity index (**RI**) and formation factor (**F**) using the Waxman-Smits equations (1968) and the B value from Juhasz (1981) to obtain $\mathbf{F^*}$, $\mathbf{RI^*}$, $\mathbf{m^*}$ and $\mathbf{n^*}$, the clay corrected cementation and saturation exponents. These clay corrections are typically less than 0.05 to **m** and 0.1 to **n**. Henceforth, we shall refer only to the "clay corrected" or geometric parameters: $\mathbf{F^*}$, $\mathbf{RI^*}$, $\mathbf{m^*}$ and $\mathbf{n^*}$.

For the distribution of $\mathbf{m^*}$, 95% of the values are between 1.7 and 2.1 with a sharp peak between 1.8-1.9. Consistent with prior observations (e.g. Wyllie and Gregory, 1953), the relatively small variation in $\mathbf{m^*}$ appears to be controlled by grain shape and cementation.

The values of $\mathbf{n^*}$ are broadly distributed between 0.6 and 2.6. The large variation in $\mathbf{n^*}$ appears to be related to cementation, pressure solution, and depositional environment (e.g. laminations).

Samples without visible laminations, as identified from thin-section photographs, have $\mathbf{n^*}$ values ranging from 1.0 to 2.6. Such samples with low values of $\mathbf{n^*}$ tend to have an appreciable fraction of their pore volumes consisting of well-connected, hairline pores. Because of their high capillarity, these pores remain brine saturated high in the hydrocarbon column and act to preserve conductivity as brine is drained from the rock.

Finely-laminated, aeolian sandstones tend to have low saturation exponents, i.e., $0.6 \leq \mathbf{n^*} \leq 1.4$. Their $\mathbf{n^*}$ values are strongly correlated to the inverse of the minimum brine saturation attained during desaturation. Such low values of $\mathbf{n^*}$ are consistent with a simple model which accounts for systematic variations in capillary pressure and brine saturation in laminated samples.

The value of $\mathbf{n^*}$ in our dataset is fairly well correlated with porosity. This correlation is useful for establishing bounds on $\mathbf{n^*}$.

CEMENTATION EXPONENTS IN CLEAN SANDSTONES

The Formation Factor (F^*) of a sample is a measure of how efficiently the pore space is distributed for electrical conduction. In the extreme of zero efficiency, if the porosity(Ø) were concentrated in a blob inside the sample with no connections to the surfaces of the sample, there would be no conduction and F^* would be infinite. Alternatively, the most efficient distribution of porosity occurs when all the pore space is concentrated in a through going tube or fracture. There the Formation Factor (F^*) would be at a minimum for that porosity and the cementation exponent m^* would be at its minimum value of 1. Any changes in cross-section of the tube or fracture would result in reduced conduction and increased F^* and m^*, assuming that the porosity remained unchanged. The porosity in most sandstones is intergranular, i.e., between the grains, and the electrical conduction paths much less uniform than through a tube. The simplest model of intergranular porosity is a bead pack. For periodic, cubic arrays of beads, Shen et al.(1990) showed that the value of m^* lies between 1.3 and 1.5. These simple structures probably have the lowest m^* values we can expect for grain supported sandstones. Most sandstones have more complicated fabrics than that of beadpacks with the consequences of higher F^* values for the same porosity and values of $m^*>1.5$. Archie (1942) found the cementation exponent to vary between 1.8 and 2.0 for consolidated sandsones. Our laboratory data are consistent with this observation.

Distribution of m* Values

The distribution of m^* values measured at Chevron is shown in histogram form as Figure 1. Almost all of the m^* values fall within the range of $m^* = 1.7$ to 2.1 and the distribution of values is sharply peaked between 1.8 and 1.9. The average value of m^* is 1.87 with a standard deviation of 0.10. The narrow range of m^* values appears to reflect a narrow range of pore geometries (as opposed to pore sizes) for these fairly "clean" sandstones.

Of the 323 samples, 164 came from Reservoir A, a Jurassic, deltaic sandstone. Samples from Reservoir A have an average m^* value of 1.89 with a standard deviation of 0.09 (Figure 2).Without samples from Reservoir A, the average value of m^* is 1.85 with a standard deviation of 0.10 (Figure 3). Thus, the average value of m^* for the complete dataset is slightly biased upward by the data from Reservoir A. Figure 4 is a crossplot of F^* versus Ø for the complete dataset.

Fabric Controls on a* and m*

When the power law relationship between Formation Factor and porosity is calculated for an individual sample, only the value of m^* can be determined (one equation, one unknown). When the power law relationship between Formation Factor and porosity is evaluated for a suite of samples, the values of both a^* and m^* are determined by regression methods. The use of two parameters (a^* and m^*) yields a better fit to the data than can be obtained with a single parameter (m^*). Typically, a^* and m^* values are determined on a suite of samples from the same formation or lithofacies. When the pore geometry is changing with porosity, the values of a^* and m^* can take on odd values as they do for the Fontainebleau sandstone. Figure 5 is a crossplot of F versus Ø for four Fontainebleau samples. Porosity ranges from 5-22% and the value of a^* is calculated to be 0.13 and m^* is 2.8.

We propose that these apparently odd values of $\mathbf{a}^*$ and $\mathbf{m}^*$ in Fontainebleau sandstones reflect increased cementation and randomly scattered large pores in the low porosity samples. Examination of the Fontainebleau samples in thin-section reveals that the higher porosity samples have minimal quartz overgrowths while the lower porosity samples have extensive quartz overgrowths (Figure 6). The $\mathbf{m}^*$ values calculated for three of the samples are shown to the right of the corresponding photomicrographs. Because cementation appears to have occurred non-uniformly, the pore sizes and pore connections in the low porosity samples are more variable in cross-section than in the high porosity samples. Note the increase in $\mathbf{m}^*$ with increasing cementation.

The increase in $\mathbf{m}^*$ due to cementation can be predicted by the grain consolidation model of Roberts and Schwartz (1985) and Schwartz and Kimminau (1987). They allow the grains to grow in the pore space of a dense random packing of spherical grains. They add a randomness to this grain growth such that not every grain undergoes cementation uniformly. The result is that grain growth reduces the porosity and changes the shape of most pores but allows some pores to remain large. This growth process results in an increase in $\mathbf{m}^*$ as porosity is decreased, due partly to the changes in pore shape and partly to the generation of "isolated" patches of porosity. The isolated patches, which occur in cemented rocks, contribute relatively little to conduction but can be a major part of the porosity.

Observing that cementation resulted in a low value of $\mathbf{a}^*$ and a high value of $\mathbf{m}^*$ for the Fontainebleau sandstone, we suggest that values of $\mathbf{a}^*<1$ are to be expected for groups of samples in which cementation is increasing with decreasing porosity. This effect may also be seen in Figure 4. There, we applied a reduced major axis (RMA) regression to all of our formation factor and porosity measurements and calculated values of $\mathbf{a}^*=0.84$ and $\mathbf{m}^*=1.97$.

SATURATION EXPONENTS IN SANDSTONES

Distribution of n* Values

The samples in this study are from 11 different oil fields and 1 quarry. Figure 7 is a histogram of $\mathbf{n}^*$ values for all of the 295 samples. The $\mathbf{n}^*$ values vary between 0.6-2.6 and exhibit a strong peak in the 2.0-2.2 range. The 295 samples include 145 Jurassic, deltaic sandstones from Reservoir A and 47 Triassic, aeolian sandstones from Reservoir B. Because these samples had a strong influence on the distribution of $\mathbf{n}^*$ values, we separated the samples into the three groups: Reservoir A sandstones, Reservoir B sandstones and sandstones from the other reservoirs.

For Reservoir A samples, the $\mathbf{n}^*$ values fall in the range of 1.4-2.6 (Figure 8) with most values between 2.0 and 2.2. For the aeolian sandstones from Reservoir B, which tend to be thinly laminated, the $\mathbf{n}^*$ values range from 0.6-1.4 (Figure 9).

When the data from Reservoirs A and B are removed (Figure 10), the distribution of $\mathbf{n}^*$ values is more uniform i.e., the strong peaks at 1.1-1.2 and 2.0-2.2 are gone. This group of samples has $\mathbf{n}^*$ values between 1.0-2.5, with the majority of $\mathbf{n}^*$ values in the range of 1.4-2.0. We infer from this data that even though a given field may have characteristic $\mathbf{n}^*$ values, these values are difficult to predict without core measurements or knowledge of the rock fabric.

Rock Fabric Effects on n*

We do not see a strong correlation between sorting and the value of **n***, based on visual estimates of sorting from thin-sections. Well-sorted samples appear just as likely to have low (or high) **n*** values as do poorly-sorted samples.

To date, 196 samples have been separated into two categories (i.e., sandstones without visible laminations and laminated sandstones) based on rock fabric from thin-section and hand specimen observations. Of the 196 samples, 75 have been identified as homogeneous. For the homogeneous samples, the **n*** values are between 1.0-2.6, with an average value of 1.92. When the homogeneous samples from Reservoir A are removed, the **n*** range does not change much (1.0-2.5), although the average value of **n*** is reduced to 1.80.

Homogeneous samples with **n*** values in the 1.0 to 1.6 range tend to be fine-grained and low porosity (<15%). Thin-section photomicrographs for two samples from this group are shown in Figure 11. These samples have a large number of hairline pores along grain contacts (apparently caused by pressure solution). We speculate that during desaturation, these pores will tend to remain brine saturated and leave a well-connected conduction path nearly as efficient as when the pores were filled with brine. However, some fine-grained, homogeneous samples with higher porosities have high **n*** values (Figure 12). Consequently, we cannot infer that a sample has a low **n*** just because it is fine-grained. Unlike the previous samples with low **n*** values, a minor fraction of the pore volume consists of well-connected, hairline pores along grain contacts. Thus, brine connections between pores will be more easily broken during desaturation with the result of higher values of **n***.

Model For the Saturation Exponent of Laminated Sandstones

The low values of $\mathbf{n}^*$ for finely laminated core are caused by variations in brine saturation from lamina to lamina within the samples. To illustrate this point, consider what happens at the same height above the oil-water contact in a sandstone with interspersed fine and coarse grained laminae, all with about the same porosity. The capillary pressure curves for the two lamina types would exhibit quite different saturations for a given capillary pressure. The fine-grained laminae will tend to have a higher brine saturation and thus be more conductive than the coarser grained laminae. The bulk resistivity of the laminated sample is the parallel (or harmonic) mean of the resistivities of the laminae weighted by their volumes, while the brine saturation is the arithmetic average of the brine saturations of the laminae (also weighted by their volumes).

For a numerical example of the lowering of $\mathbf{n}^*$ due to laminations, suppose half of a sample consists of coarse-grained laminae and half of the sample fine-grained laminae, and the formation factors and porosities of all the laminae are the same. At some height above the oil-water contact, the coarse-grained half would have a saturation of 20% and the fine-grained half a saturation of 80% (Figure 13). The average brine saturation is 50%. If both halves had a saturation exponent of $\mathbf{n}^*$=1.8, then the $\mathbf{RI}^*$s of the fine- and coarse-grained halves would be 1.49 and 18.12, respectively. The composite $\mathbf{RI}^*$, obtained by averaging the reciprocals of the $\mathbf{RI}^*$s for each half, is 2.76. The saturation exponent is obtained by using the average brine saturation of the two halves and the composite $\mathbf{RI}^*$, with the result that $\mathbf{n}^*$=1.47 for the composite. Thus, the resistivity and the saturation exponent for the composite are lower than the resistivity and saturation exponent would be for either of the

two halves at a saturation of 50%. Based on this simple analysis, then, the value of $\mathbf{n^*}$ will tend to be lower for laminated sandstones than for homogeneous sandstones.

Curvilinear RI*-Sw Crossplots for Laminated Samples

If we follow the same logic to calculate $\mathbf{RI^*}$ and $\mathbf{S_w}$ at a series of points for a laminated sample, we find that the $\mathbf{RI^*}$-$\mathbf{S_w}$ curve can no longer be represented by a simple power law relationship i.e. the $\mathbf{RI^*}$-$\mathbf{S_w}$ crossplot is no longer linear on a log-log plot, but can exhibit significant curvature.

Figure 14 is a plot of $\mathbf{RI^*}$ versus $\mathbf{S_w}$ for two laminated samples. These data exhibit the most curvature we have seen in $\mathbf{RI^*}$-$\mathbf{S_w}$ plots. Note that at high brine saturations, the slope of the crossplotted data is low (low $\mathbf{n^*}$ value), while at lower brine saturations the slope is steeper (larger $\mathbf{n^*}$). Thus, if similar samples are desaturated to only 60-70%, they will appear to have low $\mathbf{n^*}$ values. This condition of high minimum brine saturation occurs for low permeability, laminated samples from Reservoir B. These samples require higher capillary pressures to drive them to low brine saturations than are provided by the thickness of the hydrocarbon column. Such samples are, consequently, desaturated only to fairly high brine saturations and exhibit low values of $\mathbf{n^*}$. In Figure 15, we crossplotted the clay-corrected saturation exponent $\mathbf{n^*}$ versus the minimum brine saturations attained in the finely-laminated samples from Reservoir B. Note the trend toward higher values of $\mathbf{n^*}$ for low, minimum brine saturations. This trend is consistent with the curvature in the $\mathbf{RI^*}$-$\mathbf{S_w}$ plot of Figure 14.

Photo-micrographs of Laminated Samples with Low Saturation Exponents

Figures 16-17 are photomicrographs of thin-sections of laminated, aeolian sandstones from Reservoir B. The figures are annotated with the values of $\mathbf{n^*}$ measured on each sample. The sample with the higher $\mathbf{n^*}$ value (Figure 16) has essentially two grain sizes, i. e. laminae of either fine grains or medium grains. This geometry has resulted in a moderate contrast in capillarity between the laminae. Consequently, both types of lamina could be desaturated to fairly low brine saturations and there was only a moderate lowering of the value of $\mathbf{n^*}$ calculated from the $\mathbf{RI^*}$-$\mathbf{S_w}$ crossplot.

The sample with the lower $\mathbf{n^*}$ value (Figure 17) has a lower average grain size and broader distribution of grain sizes in the laminae. The laminae tend to be either medium-grained and well-sorted or poorly sorted with grain sizes ranging from extremely fine-grained to medium-grained. This sample has a large contrast in capillarity between the laminae such that the poorly sorted laminae probably remained fully brine saturated at even the highest capillary pressures used to desaturate the sample. Consequently, the minimum brine saturation attained during desaturation was high and the value of $\mathbf{n^*}$ low.

Correlations of n*_with Porosity

Figure 18 shows that there is a fair trend between $\mathbf{n^*}$ and $\mathbf{\emptyset}$ in the Chevron dataset. Although the correlation is not strong enough to build a reliable estimate of $\mathbf{n^*}$ from porosity, there are useful bounds which we can put on $\mathbf{n^*}$ for a given porosity. The apparent trend between $\mathbf{n^*}$ and $\mathbf{\emptyset}$ has significant economic implications. In higher porosity formations, the calculated brine saturation will not vary much whether $\mathbf{n^*}$ is 2 or 2.5. However, in low porosity formations, where a low initial brine saturation is usually required for the field to be economic, knowing whether $\mathbf{n^*}$ is 1 or 2 can be critical to the

economic evaluation of the field. For example, if RI^*=5, then S_w=20% for n^*=1 and S_w=45% for n^*=2.

DISCUSSION

Summary

The electrical properties data presented represent more than 15 years of measurements made in the same laboratory at Chevron. The cementation exponent m^* is seen to vary over a narrow range of values while the saturation exponent n^* varies over a wide range. We inferred that pore shape is the major factor controlling m^* and that pore shape, pore size and heterogeneities such as laminations can all exert significant controls on n^*. We found that laminations could cause n^* values to be low in a predictable way, but also found that apparently homogeneous samples could have low n^* values. These samples with low n^* values tend to have low porosities and a high percentage of their pore volumes consisting of hairline pores along grain boundaries. We believe that these small pores remain brine saturated and well connected at the capillary pressures normally encountered in a reservoir. This leads to low n^* values. We have a fair correlation between n^* and Ø to set bounds on the range of possible values of n^*. However, we do not yet have a general formula for accurately predicting n^* in clean sandstones.

As shown herein, by Swanson (1985), and by Worthington and Pallatt (1990), heterogeneous sandstone plugs with spatially variable capillary pressures and brine saturations, cannot be expected to exhibit simple power law behavior, i.e., the RI^* versus S_w crossplots may not appear linear on log-log plots. For a curvilinear RI^* versus S_w response, it may be necessary to use another functional form or a lookup table to determine S_w from well log estimates of RI^*.

ACKNOWLEDGEMENTS

All of the data in this report were obtained using the laboratory equipment and procedures developed by Pat Worthington. Most of the measurements were made under his direction. Pat, who retired in 1988, left us with a wealth of well documented, high quality data to analyze as well as a smoothly functioning laboratory. We appreciate his contributions and dedicate this paper to him.

We thank Jim Spencer of Chevron for his careful review of this paper and his useful insights into the significance of the effects of pressure solution on the saturation exponents of low porosity sandstones. We also thank the management of Chevron for their support and permission to publish this paper.

REFERENCES

Archie, G. E., The Electrical Resistivity Log as an Aid in Determining Some Reservoir Characteristics, Trans. AIME, 146, pp54-62, 1942.

Baldwin, B. A. and Yamanashi, W. S., Persistence of Non-Uniform Brine Saturation Distribution in SCA Electrical Resistivity Core Plugs After Desaturation by Centrifuging, The Log Analyst, Vol. 30, No. 2, pp45-48, 1989.

Juhasz, I., Normalised Q_v - The Key to Shaly Sand Evaluation Using the Waxman-Smits Equation in the Absence of Core Data, Transactions SPWLA Twenty-Second Annual Logging Symposium, Paper Z, 1981.

Roberts, J. N., and Schwartz, L. M., Grain Consolidation and Electrical Conductivity in Porous Media, Phys. Rev., B31, pp5990-5997, 1985.

Schwartz, L. N., and Kimminau, S., Analysis of Electrical Conduction in the Grain Consolidation Model, Geophysics, Vol. 52, No. 10, pp1402-1411, 1987.

Shen, L. C., Liu, C., Korringa, J., and Dunn, K. J., Computation of Conductivity and Dielectric Constant of Periodic Porous Media, J. Appl. Phys. Vol. 67, No. 11, pp7071-7081, 1990.

Swanson, B. F., Microporosity in Reservoir Rocks - Its Measurement and Influence on Electrical Resistivity, Transactions SPWLA Twenty-Sixth Logging Symposium, Paper F, 1985.

Waxman, M. H., and Smits, L. J. M., Electrical Conductivities in Oil-Bearing Shaly Sands, SPE Journal, Vol. 8, pp107-122, 1968.

Worthington, P. F., and Pallatt, N., Effect of Variable Saturation Exponent Upon the Evaluation of Hydrocarbon Saturation, Transactions of SPE Sixty-Fifth Technical Conference, pp101-108, 1990.

Wyllie, M. R. J., and Gregory, A. R., Formation Factors of Unconsolidated Porous Media: Influence of Particle Shape and Effect of Cementation, Trans. AIME, 198, pp103-111, 1953.

APPENDIX: POTENTIAL MEASUREMENT ERRORS

There are potential sources of error in our saturation exponent measurements which are not fully resolved.

First, all of the measurements of $\mathbf{RI^*}$ versus S_w were done using horizontal and angle head centrifuges to lower the brine saturation in the samples. Our concern with using the centrifuge for desaturation is that non-uniform brine distributions can be established. The end of the plug further from the center of rotation will have a higher brine saturation than the end closer to the center. The use of an angle head centrifuge, where the samples are at a 45° angle to the rotation axis, further complicates the brine distribution. After the samples are removed from the centrifuge, this non-uniform saturation can persist for much longer times than originally thought (Baldwin and Yamanashi, 1989). The effect of non-uniform saturations along the length of the samples is to cause the samples to appear more resistive than they would have if the same amount of brine were uniformly distributed. We saw such an effect in chalk samples during the early 80's but were unable to determine its cause at the time. The chalks we studied possessed low permeabilities and high porosities. At the lowest centrifuge speed, a non-uniform saturation was apparently established that persisted throughout successive desaturations. The crossplots of $\mathbf{RI^*}$ versus S_w were peculiar in that the first desaturation point at S_w = 80-90% had a higher than expected value of $\mathbf{RI^*}$, but the successive points followed the usual power law behavior, i.e., fell on a straight line in the log-log crossplot. We did not see a significant tendency for this type of

behavior in our sandstone data. Still, we cannot be completely confident that our n^* values are not slightly overestimated, especially for low permeability samples.

Second, all our samples were solvent-cleaned using successively toluene, methanol and an 80/20% azeotrope of chloroform and acetone. Though not regularly tested for wettability, these samples were presumed to be strongly water-wet. Our concern is that in the reservoir, the samples may have been significantly less water-wet (i.e. larger contact angle) which would alter the brine distribution and would increase, to some unknown degree, the saturation exponent, n^*.

Third, we are concerned that the tendency of our low porosity samples to have low saturation exponents could be due to a measurement artifact. At low brine saturations, the amount of brine in samples with 10% porosity is only about 0.3 milliliters. Brine saturation is determined from weights and knowledge of the density of the brine. Any evaporation of water, will be seen as a reduction in brine saturation, but will leave the remaining brine more saline so that the resistivity will not increase as it would if both salt and water were removed. The result is a lower value of RI^* at that saturation and a consequent lowering of the value of n^*. Although evaporation is clearly a source of error during air/brine desaturation, we expect possible errors of only 0.1 or 0.2 in the value of n^*. This is based on our analysis of the following worst case example. From weights, we estimated that a sample had been desaturated to the extremely low value of $S_w = 0.01$, where some loss due to evaporation would be expected. The amount of salt remaining in the sample, as determined using an Inductively Coupled Plasma (ICP) spectrometer, was twice what we calculated assuming no evaporation. This meant that the brine saturation was slightly off and resistivity was low by a factor of two. Correcting the resistivities and brine saturations, however, changed the calculated value of n^* by less than 0.2. Thus, while the possibility of evaporation raises a question about the accuracy of RI^* measurements on low porosity samples, evaporation effects do not appear large enough to account for the strong tendency for low porosity samples to have low n^* values.

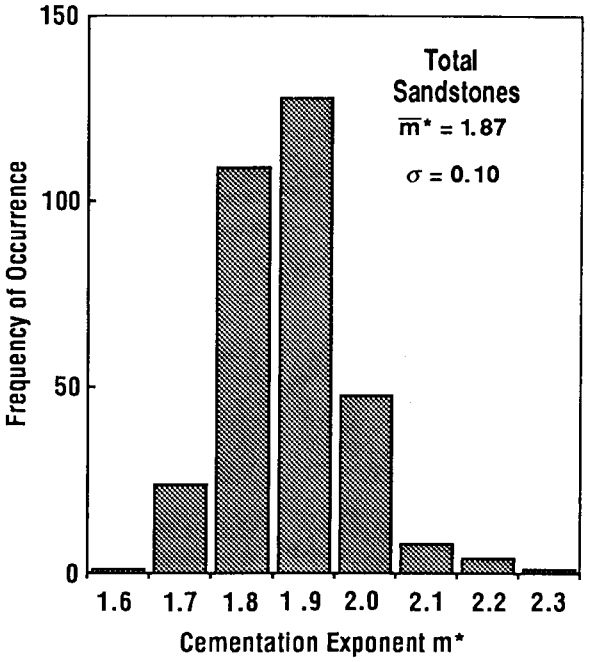

Figure 1 Data for total (11) Reservoirs.

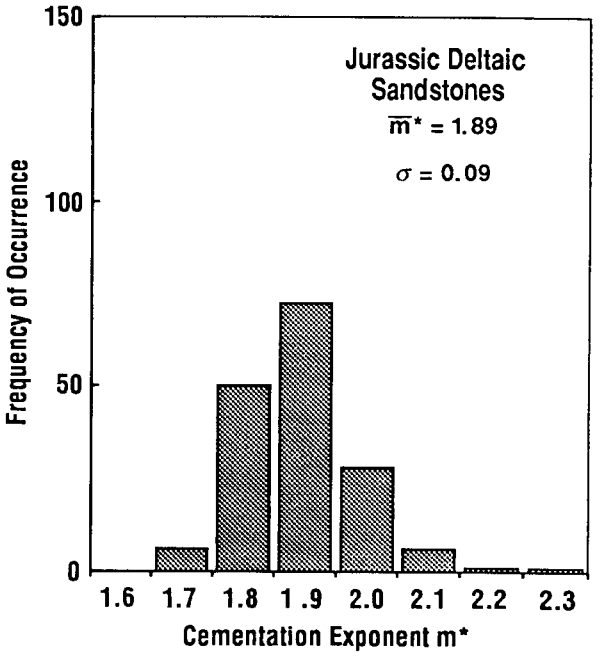

Figure 2 Reservoir A data.

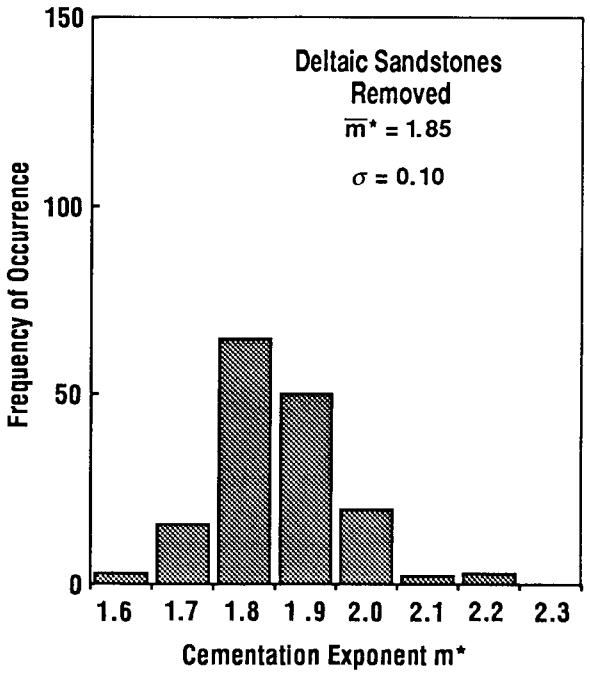

Figure 3 Total data with Reservoir A data removed.

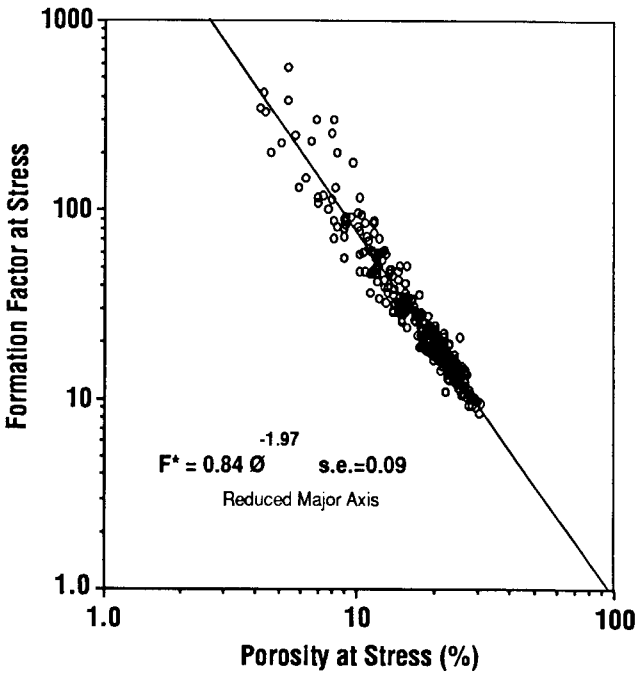

Figure 4 Formation factor versus porosity for Chevron samples.

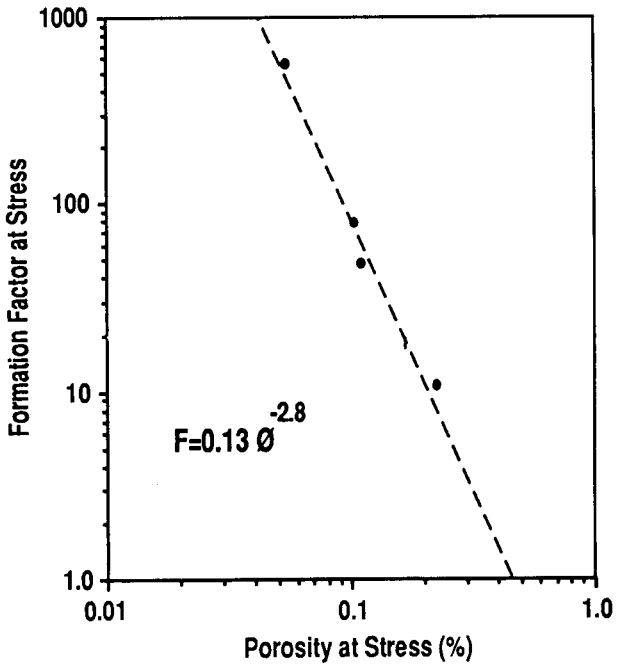

Figure 5 Crossplot of Formation Factor versus porosity for Fontainebleau sandstone.

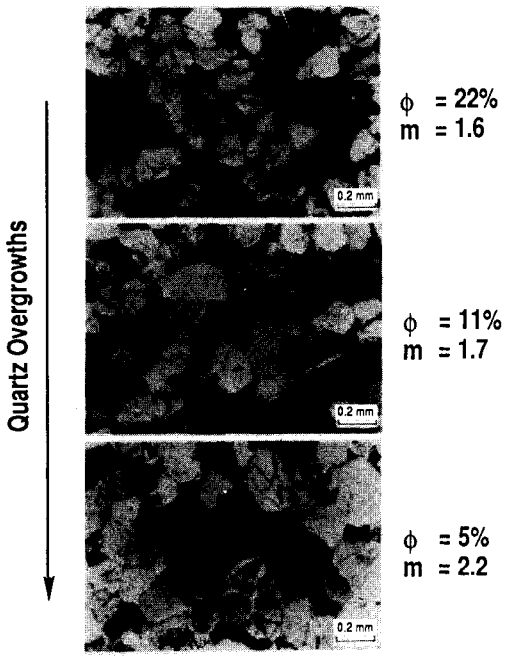

Figure 6 Quartz overgrowths lead to higher m* values.

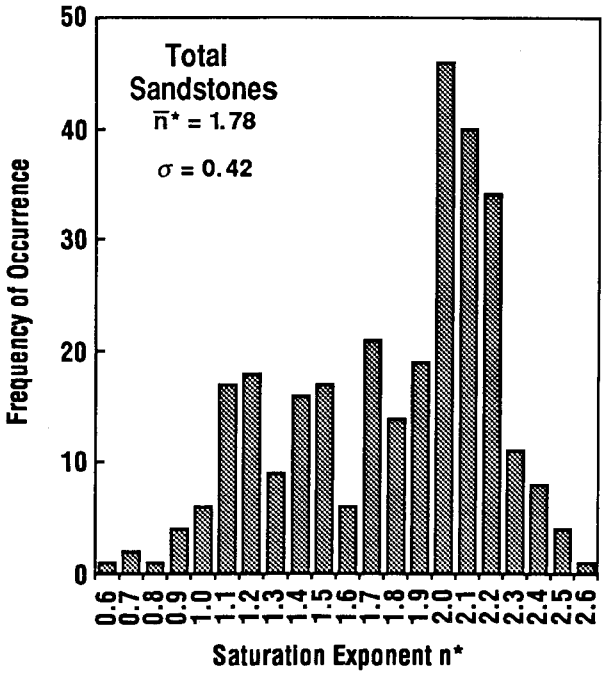

Figure 7 Data for total (11) Reservoirs.

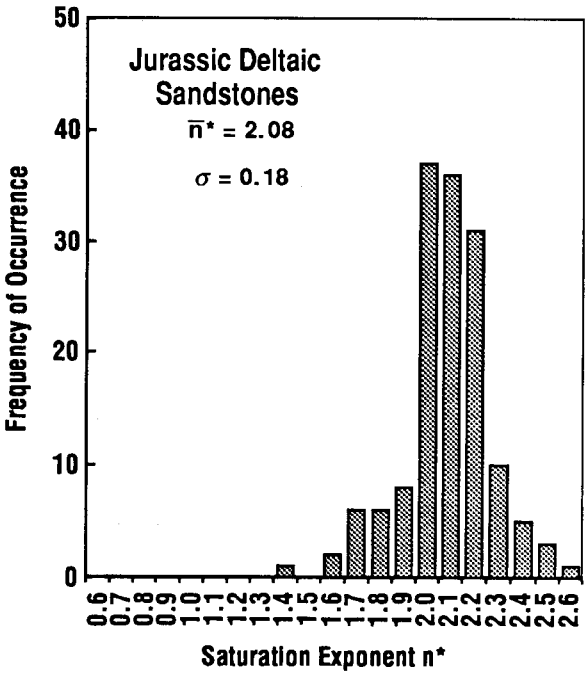

Figure 8 Reservoir A data.

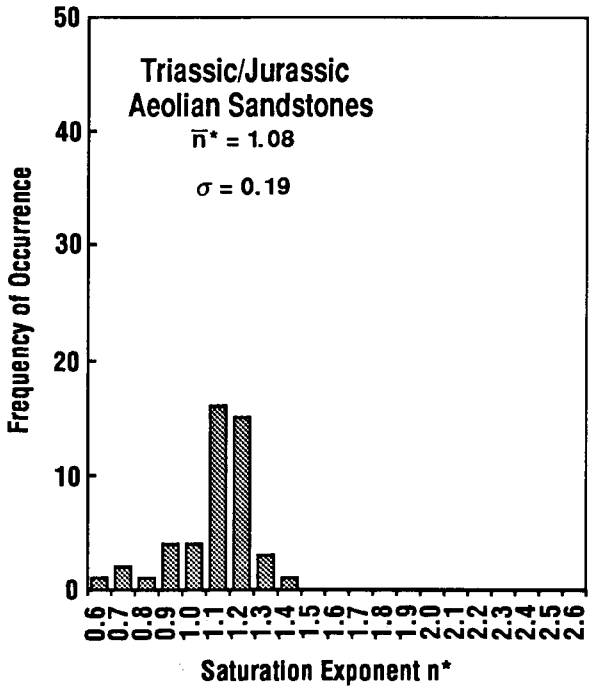

Figure 9 Reservoir B data.

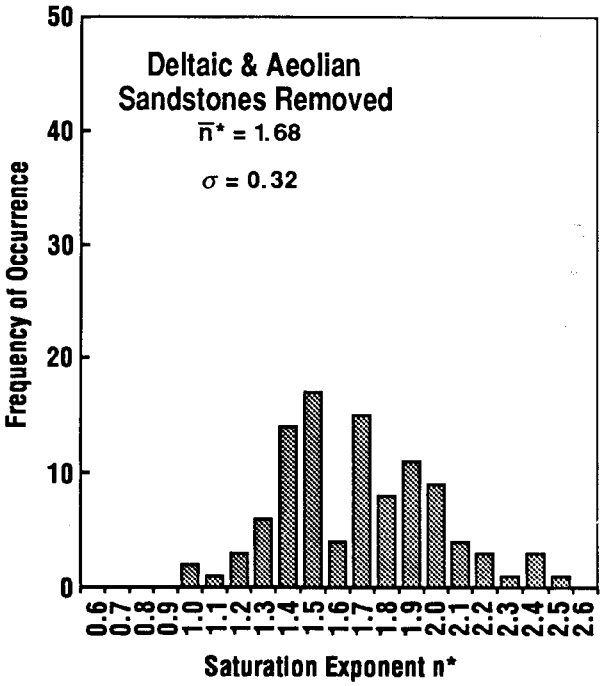

Figure 10 Reservoirs A & B data removed.

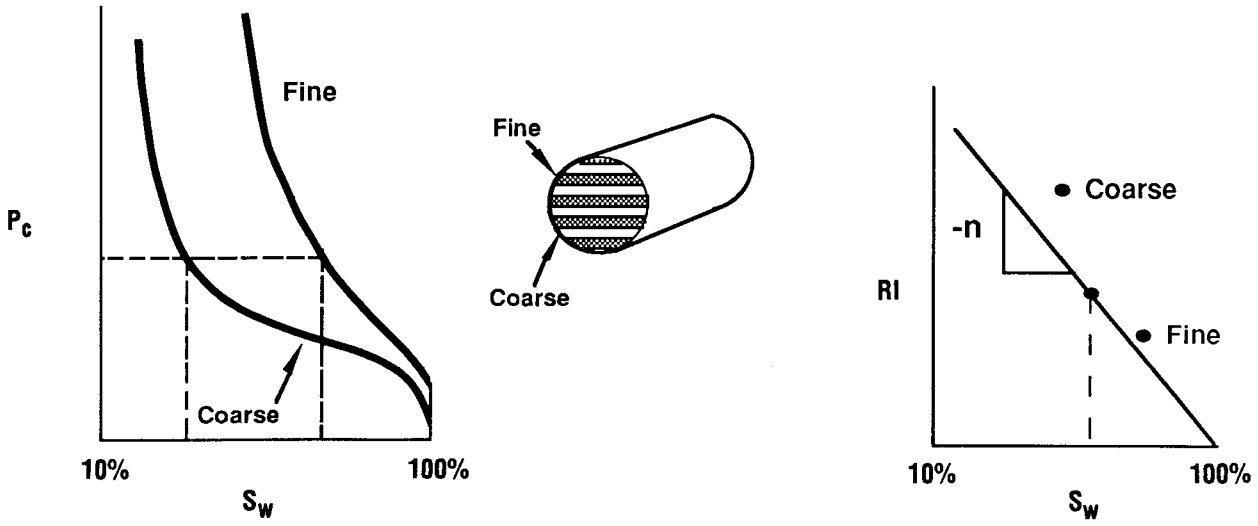

Figure 13 Laminations can lead to low values of saturation exponent n*.

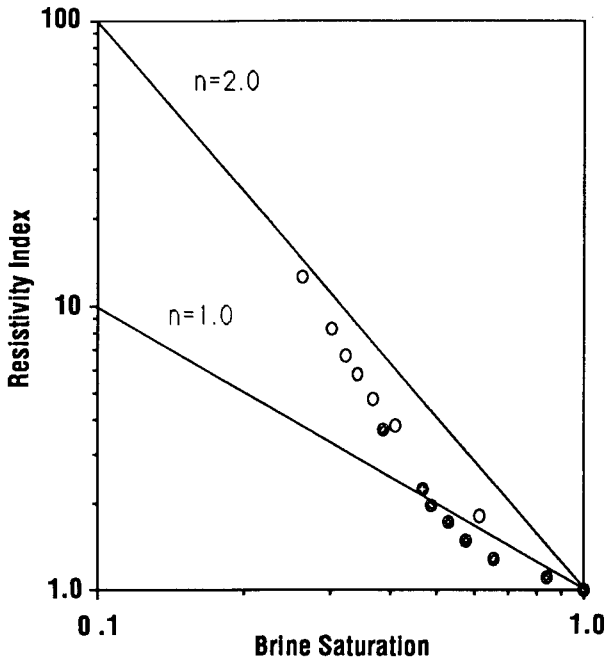

Figure 14 Resistivity Index versus brine saturation data for two laminated sandstones exhibit curvature.

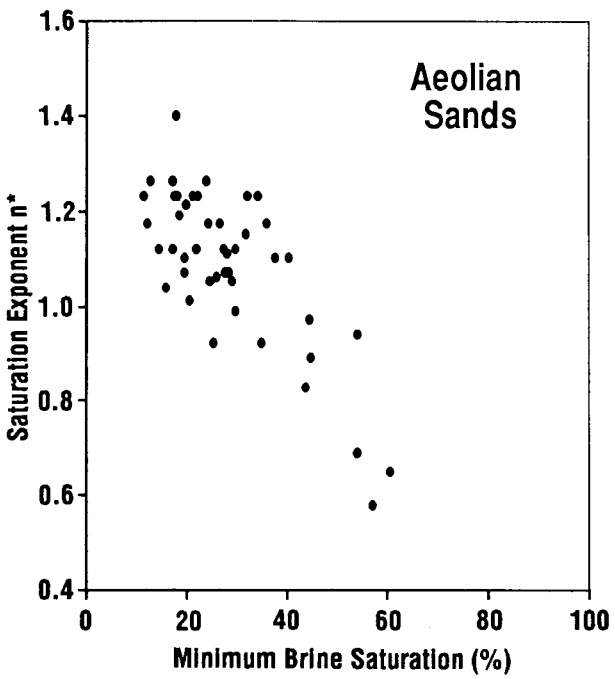

Figure 15 In aeolian sands, low values of n* tend to be associated with high values of minimum brine saturation.

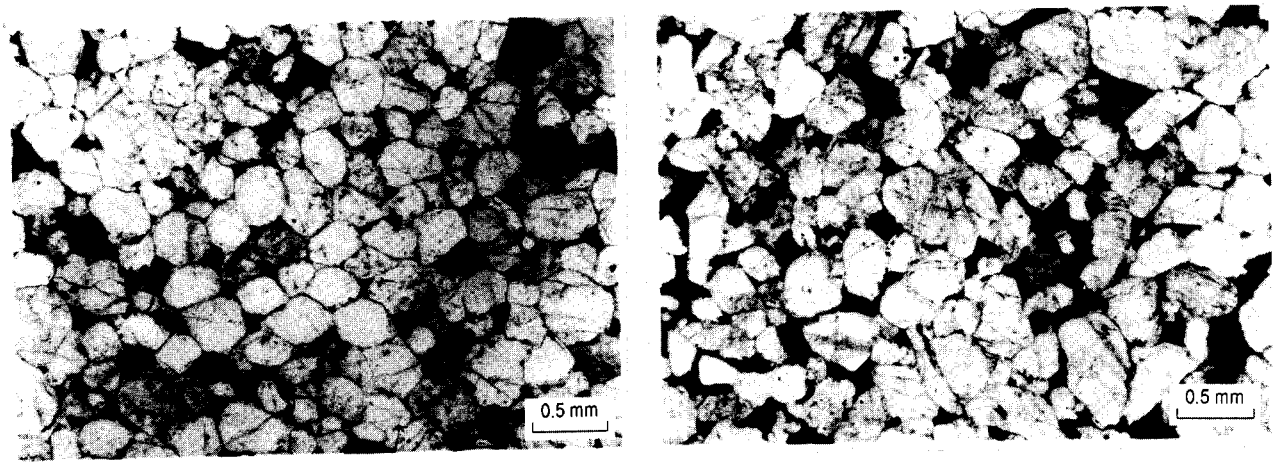

n* = 1.13
ø = 8%

n* = 0.98
ø = 11%

Figure 11 Fine-grained homogeneous sandstones with low n* values.

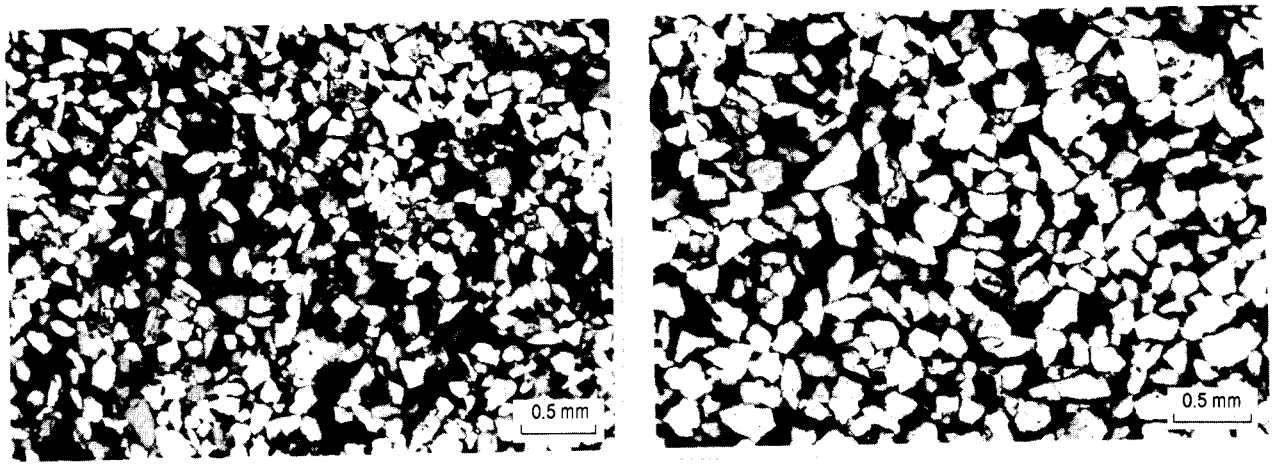

n* = 2.14
ø = 30%

n* = 2.64
ø = 25%

Figure 12 Fine-grained homogeneous sandstones with high n* values.

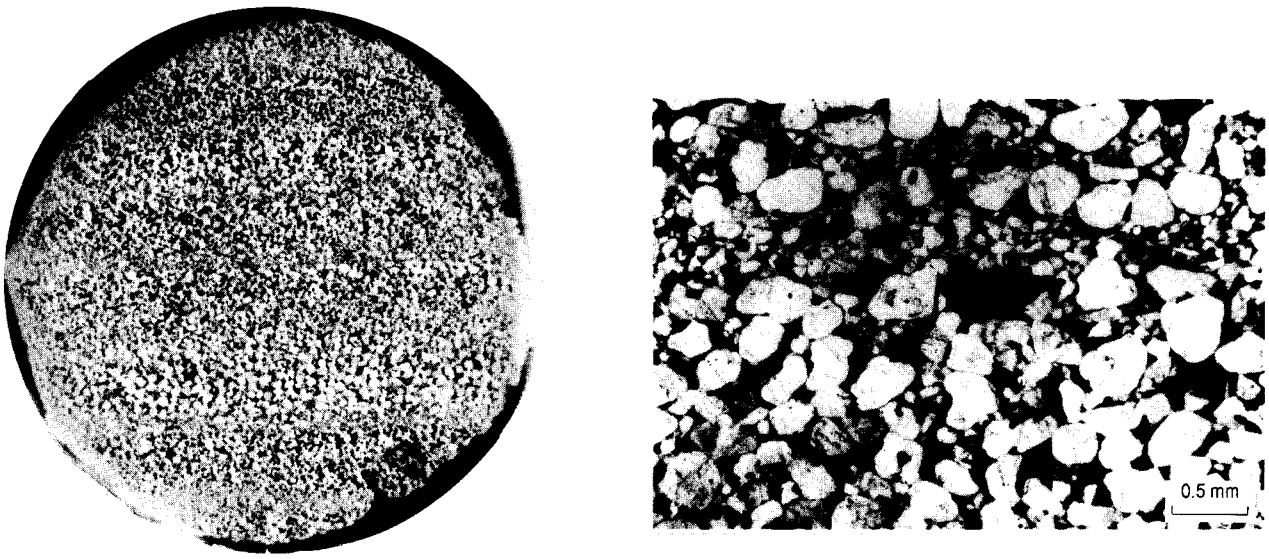

$n^* = 1.40$
$K_a = 18$ md

Figure 16 Fine to medium-grained aeolian sandstone with well-sorted laminae.

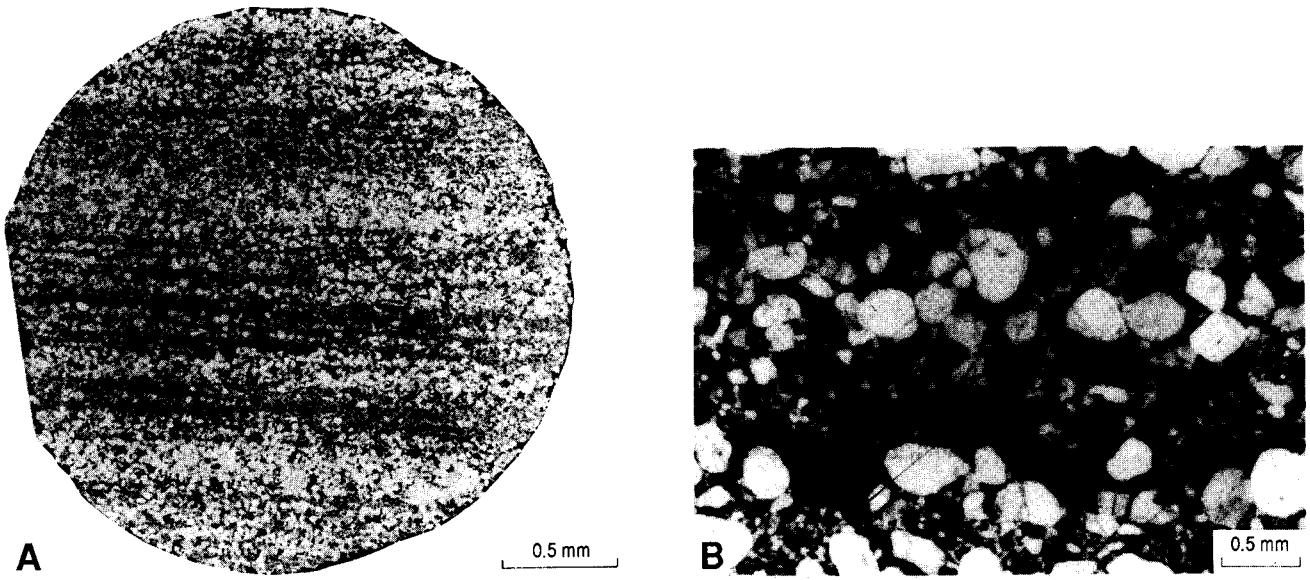

$n^* = 0.65$
$K_a = 0.09$ md

Figure 17 Very fine to medium-grained aeolian sandstone with poorly-sorted laminae.

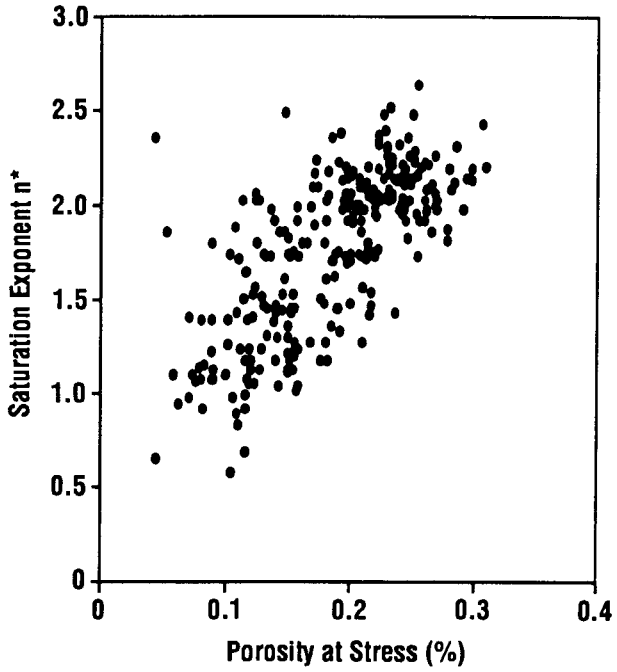

Figure 18 For the Chevron data, there is a fair correlation between porosity and n*.